LETTER

Senescence–associated reprogramming promotes cancer stemness

Maja Milanovic[1], Dorothy N. Y. Fan[1,2,3,4], Dimitri Belenki[1], J. Henry M. Däbritz[1], Zhen Zhao[5], Yong Yu[6], Jan R. Dörr[1], Lora Dimitrova[7], Dido Lenze[7], Ines A. Monteiro Barbosa[8], Marco A. Mendoza-Parra[9], Tamara Kanashova[6], Marlen Metzner[1], Katharina Pardon[1], Maurice Reimann[1], Andreas Trumpp[2,3,4,10], Bernd Dörken[1,2,4,6,11], Johannes Zuber[8], Hinrich Gronemeyer[9], Michael Hummel[2,4,7,11], Gunnar Dittmar[6,12], Soyoung Lee[1,2,4,6] & Clemens A. Schmitt[1,2,4,6,11]

Cellular senescence is a stress-responsive cell-cycle arrest program that terminates the further expansion of (pre-)malignant cells[1,2]. Key signalling components of the senescence machinery, such as p16[INK4a], p21[CIP1] and p53, as well as trimethylation of lysine 9 at histone H3 (H3K9me3), also operate as critical regulators of stem-cell functions (which are collectively termed 'stemness')[3]. In cancer cells, a gain of stemness may have profound implications for tumour aggressiveness and clinical outcome. Here we investigated whether chemotherapy-induced senescence could change stem-cell-related properties of malignant cells. Gene expression and functional analyses comparing senescent and non-senescent B-cell lymphomas from Eμ-Myc transgenic mice revealed substantial upregulation of an adult tissue stem-cell signature, activated Wnt signalling, and distinct stem-cell markers in senescence. Using genetically switchable models of senescence targeting H3K9me3 or p53 to mimic spontaneous escape from the arrested condition, we found that cells released from senescence re-entered the cell cycle with strongly enhanced and Wnt-dependent clonogenic growth potential compared to virtually identical populations that had been equally exposed to chemotherapy but had never been senescent. In vivo, these previously senescent cells presented with a much higher tumour initiation potential. Notably, the temporary enforcement of senescence in p53-regulatable models of acute lymphoblastic leukaemia and acute myeloid leukaemia was found to reprogram non-stem bulk leukaemia cells into self-renewing, leukaemia-initiating stem cells. Our data, which are further supported by consistent results in human cancer cell lines and primary samples of human haematological malignancies, reveal that senescence-associated stemness is an unexpected, cell-autonomous feature that exerts its detrimental, highly aggressive growth potential upon escape from cell-cycle blockade, and is enriched in relapse tumours. These findings have profound implications for cancer therapy, and provide new mechanistic insights into the plasticity of cancer cells.

Cellular senescence, which is implemented in response to severe cellular insults such as oncogenic activation or chemotherapeutic DNA damage, is a failsafe program that protects organismic integrity by excluding potentially harmful cells from further expansion[2,4], and also has a physiological function in tissue homeostasis during organ development[1]. Senescence has been shown to cancel the pro-tumorigenic potential of Ras-/Raf-driven (pre-)cancerous lesions[5–7], and to contribute to the outcome of anticancer chemotherapy in vivo[8,9].

Notably, stem-cell functions, collectively referred to as 'stemness'[3], and senescence seem to be co-regulated by overlapping signalling networks. Key senescence-relevant signalling molecules (for example, Bmi-1, p16[Ink4a], p21[Cip1] or p53) have critical roles in stem-cell maintenance by preventing premature exhaustion (reviewed in ref. 3). Senescence-enforcing p53 (also known as Trp53)-, Cdkn2a (also known as Ink4a or Arf)- or Suv39h1-encoded gene products raise an initial barrier to the efficient conversion of normal cells into induced pluripotent stem cells (see refs 10, 11, and references therein), suggesting an underexplored interplay between senescence- and stemness-controlling signalling networks. Trimethylation of H3K9, as mediated by the H3K9 methyltransferase Suv39h1 (ref. 12), confers senescence by establishing a transcriptionally repressive heterochromatin mark in the vicinity of S-phase-relevant E2F target genes[6,9,13], and reflects an epigenetic principle linked to induced pluripotent stem cell reprogramming[14]. Using a cancer-unrelated, inducible reprogramming mouse model in which many cells primarily senesced, previous studies have shown that factors secreted from these senescent cells facilitated the reprogramming of their neighbours[15,16]. Whether the senescence condition promotes cancer stemness, especially in a cell-autonomous manner, is not known. Although a permanent senescent cell-cycle block is per se incompatible with self-renewal, we report here the senescence-evoked cell-intrinsic reprogramming of cancer cells into a stem-like state, and the acquisition of tumour-initiating potential after their forced release or spontaneous escape from a chemotherapy-induced senescent cell-cycle arrest.

As indicated by their strong senescence-associated β-galactosidase (SA-β-gal) activity and other previously demonstrated markers of senescence, primary Eμ-Myc transgenic Bcl2-overexpressing lymphomas (hereafter referred to as control;Bcl2 lymphomas) serve as a well-established model for therapy-induced senescence (TIS)[8,9]. First, we analysed stem-cell-related transcripts in the gene expression profiles of 12 matched pairs of primary control;Bcl2 lymphomas that either entered TIS after in vitro exposure to the chemotherapeutic agent Adriamycin (ADR) or remained untreated. Using gene set enrichment analysis (GSEA), a previously established adult tissue stem-cell (ATSC) signature[17] was strongly skewed towards the TIS group, but was not found to be enriched in the equally ADR-treated but senescence-incapable group of Suv39h1-deficient Eμ-Myc;Bcl2 (that is, Suv39h1−;Bcl2) lymphomas[9] (Fig. 1a and Extended Data Fig. 1a, b). Almost the entire population turned double-positive for the stem-cell antigen Sca1 and the senescence marker H3K9me3 upon senescence induction (Fig. 1b, top). Furthermore, TIS cells, unlike non-senescent
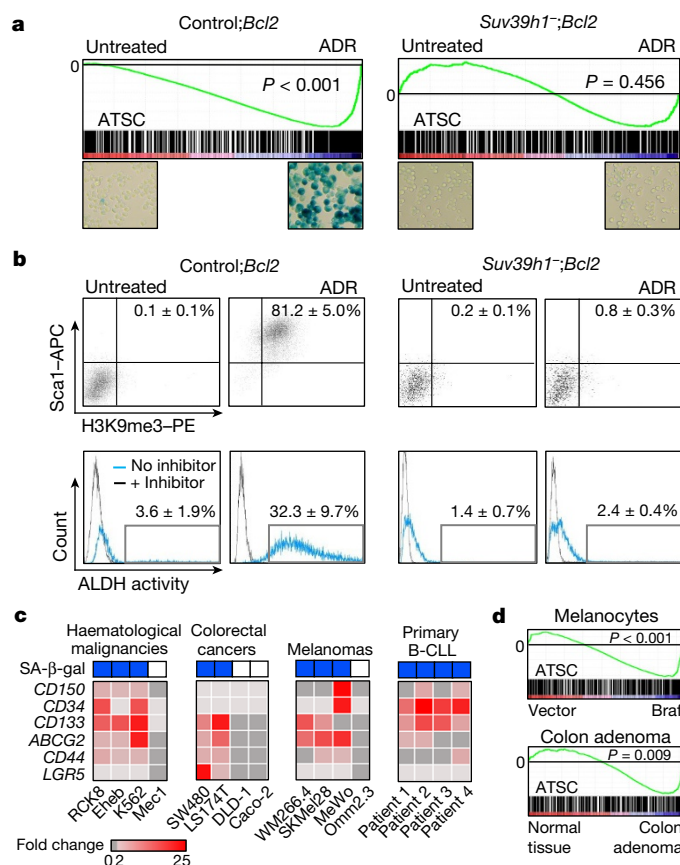
Figure 1 | Therapy-induced senescent cancer cells acquire phenotypic and functional stemness features. a, GSEA of an adult tissue stem cell profile[17] (ATSC; top) in matched pairs of ADR-exposed versus untreated control;*Bcl2* lymphomas ($n = 12$; left) and *Suv39h1*[−];*Bcl2* lymphomas ($n = 5$; right). TIS lymphomas display more than 80% SA-β-gal-positive blue cells[9] (representative photomicrographs from four independent experiments). b, Co-expression of the stem cell marker Sca1 and the TIS marker H3K9me3 (top) in lymphoma cells as in a, and aldehyde dehydrogenase (ALDH) activity with and without the ALDH inhibitor diethylaminobenzaldehyde (bottom) by flow cytometry. Mean percentage of positive cells ± s.d.; $n = 5$ biologically independent samples each. c, Expression of the indicated stem-cell-related genes in various human cancer cell lines or primary B-CLL samples by quantitative PCR (qPCR), related to their ability to enter TIS (ADR-senescent, blue; non-senescent despite ADR exposure, white (see Extended Data Fig. 1c for details)). Colours reflect fold induction (between ADR-treated and untreated samples) from one representative out of three independent experiments (cell lines) or four individual samples from patients with B-CLL. Transcripts below the detection level are shown in light grey. d, GSEA of the adult tissue stem-cell profile in the publicly available transcriptome of *BRAF*[V600E]-infected melanocytes, which senesce in response to Braf activation[7,28] (left; seven matched pairs), and colon adenomas, which are known to contain a large proportion of senescent cells[29] (right; five *Apc*[Min/+] mouse adenoma biopsies and six healthy colon tissue samples).

cells, presented with increased aldehyde dehydrogenase (ALDH) and ATP-binding cassette (ABC) transporter activities (Fig. 1b, bottom, and Extended Data Fig. 1d), both typical properties of stem cells. When assessing human malignancies of various origins, we found a notable upregulation of stem-cell-related transcripts selectively in TIS-capable cell lines as well as samples from patients with primary B-cell chronic leukaemia (B-CLL) (Fig. 1c and Extended Data Fig. 1c, e, f). Moreover, the acquisition of stemness-related properties can also be found in the process of oncogene-induced and replicative senescence in cells of various tissue types, including melanocytes, colon mucosa and breast epithelial cells (Fig. 1d and Extended Data Fig. 1g). Hence, cancer cells
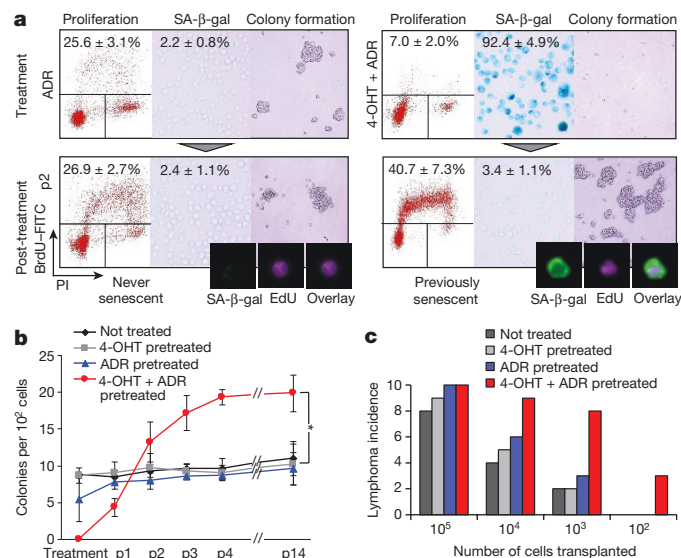

Figure 2 | Senescence-released (previously senescent) lymphomas display higher tumour-initiating capacity than their never senescent counterparts. a, Growth properties of conditionally senescent *Suv39h1*[−];*Bcl2;Suv39h1*-ER[T2] lymphoma cells after five days of ADR ± 4-OHT treatment (treatment), and subsequent passages in 4-OHT/ADR-free medium (post-treatment, p1–p2; each passage reflecting seven days in culture) presented as proliferation (left, mean BrdU/PI-marked S-phase fraction ± s.d., $n = 5$ biologically independent samples; BrdU, 5-bromo-2′-deoxyuridine; PI, propidium iodide), SA-β-gal staining (middle, mean positive cells ± s.d., $n = 5$ biologically independent samples), and colony formation (right, quantified in b). Flow microscopy images (bottom) of the fluorescent SA-β-gal mark together with the proliferation marker EdU (passage 1 shown, see Extended Data Fig. 2g for details) demonstrates the outgrowth of senescent (SA-β-gal^{+}) cells. Representative photomicrographs from four independent experiments. b, Colony counts of lymphoma cells (treated as in a) in extended serial passaging (p1–p14). Graphs show mean colony numbers ± s.d., $n = 3$ individual lymphomas. Two-tailed unpaired t-test with Welch's correction, comparing ADR- and 4-OHT+ADR pretreated cells at p14. *$P < 0.05$. c, Tumour initiation after transplantation of different numbers of *Suv39h1*[−];*Bcl2;Suv39h1*-ER[T2] lymphoma cells pre-exposed to the indicated treatments *in vitro*. Bars reflect numbers of lymphoma-bearing mice out of 10 animals per group transplanted, within an observation period of up to 100 days. $P < 0.001$ for comparing never senescent and previously senescent groups (χ^2).

of mouse and human origin acquire novel stem-cell features upon entering cellular senescence.

To test whether senescence-associated stemness (SAS) translates into different tumour behaviour upon release from the division block, we generated switchable model systems (using 4-hydroxytamoxifen (4-OHT)-inducible essential senescence mediators Suv39h1 or p53) that can enter full-featured senescence with increased levels of stem-cell-related transcripts and proteins only when exposed to both 4-OHT and ADR (Fig. 2a and Extended Data Fig. 2a–c). After changing to ADR- and 4-OHT-free medium to switch Suv39h1 or p53 off again, single-cell analyses revealed that senescent cells resumed sustainable proliferation within a few days; that is, they became first double-positive for the retained fluorescence-based senescence marker (a vital stain) and 5-ethynyl-2′-deoxyuridine (EdU) incorporation, indicating restarted DNA synthesis (with the proliferation-repressive H3K9me3 mark gradually vanishing), before SA-β-gal activity was eventually lost and S-phase activity fully regained (Fig. 2a and Extended Data Fig. 2d–g). Therefore senescence is, in principle, a reversible condition, which becomes evident when essential senescence maintenance genes are no longer expressed. Importantly, serial replatings in colony-formation experiments of such previously senescent cells led to signi-ficantly more colonies compared to the aliquot of never senescent cells
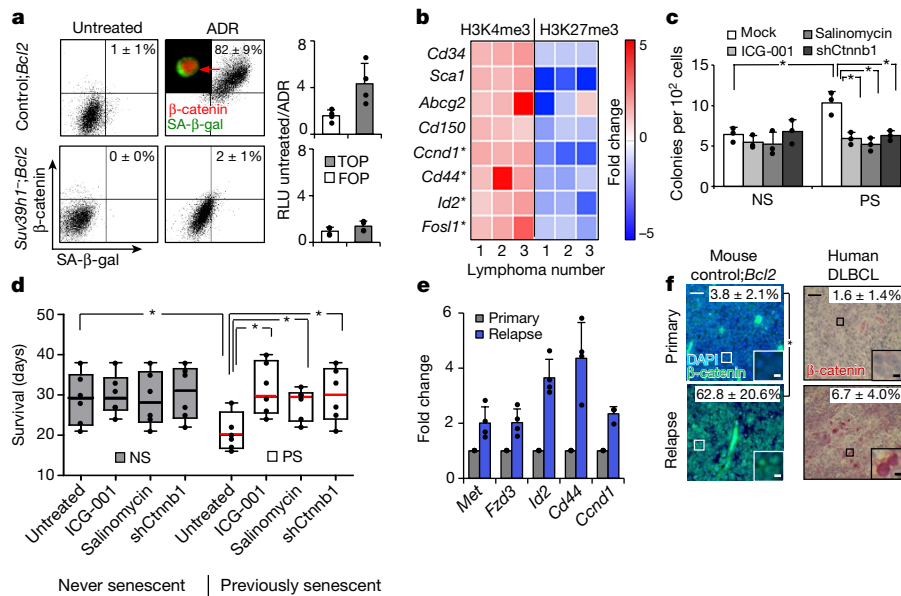
Figure 3 | Canonical Wnt signalling, activated in TIS, is an essential driver of the enhanced tumour initiation capacity exhibited by senescence-released tumour cells. a, Co-expression of the fluorescent SA-β-gal marker and β-catenin in ADR-exposed control;*Bcl2* or TIS-incapable *Suv39h1⁻;Bcl2* lymphoma cells (left), and corresponding β-catenin transcriptional activities measured as relative TOPflash T-cell factor (TCF) reporter signals with FOPflash as a TCF-binding site mutant control (right). Mean percentage of double-positive cells or mean relative light units fold change (between ADR-treated and untreated samples) ± s.d., respectively ($n = 4$ biologically independent samples each). The inset shows a representative photomicrograph from four independent experiments. **b**, Colour-coded heat map reflecting fold change (between previously senescent and never senescent cells) of permissive H3K4me3 and repressive H3K27me3 histone marks at the promoters of indicated ATSC- or Wnt-related (asterisks) genes by chromatin immunoprecipitation ($n = 3$ biologically independent samples). **c**, Colony formation of never senescent (NS) versus previously senescent (PS) *Suv39h1⁻;Bcl2;Suv39h1*-ER^T2 lymphomas (passage 2, compare with Fig. 2), exposed to the pharmacological Wnt inhibitors (ICG-001, salinomycin) or

shRNA against *Ctnnb1* (shCtnnb1) for 7 days. Results reflect mean colony numbers ± s.d. ($n = 3$ biologically independent samples). Two-tailed unpaired *t*-test with Welch's correction, $*P < 0.05$. **d**, Survival of mice transplanted with matched previously senescent or never senescent cells and treated with indicated Wnt inhibitors upon palpable lymphoma formation. Cells with shRNA against *Ctnnb1* were shRNA-infected before transplantation. Boxes frame the 25th to 75th percentile range, with median, minimal and maximal values ($n = 6$ mice per treatment group). Two-tailed, paired *t*-test, $*P < 0.05$. **e**, Expression of Wnt target genes (by qPCR) in matched cases of control;*Bcl2* lymphomas before and after relapse from senescence-inducing cyclophosphamide treatment *in vivo* (mean fold change ± s.d., $n = 4$ biologically independent samples). **f**, Nuclear β-catenin expression by immunostaining of lymph nodes from control;*Bcl2* lymphoma-bearing mice as in **e** (left; $n = 4$ biologically independent samples), and human DLBCL biopsies from the same individual patients at diagnosis and at relapse after first-line induction chemotherapy (right; $n = 5$ independent patients). Mean percentage of positive cells ± s.d.; two-tailed, paired *t*-test, $*P < 0.05$. Representative photomicrographs; scale bars, 100 μm (magnifying inserts, 10 μm).

of the same lymphoma treated with the same dose of chemotherapy, reflecting the now unleashed stemness properties acquired as a latent program during senescence (Fig. 2a, b). The enhanced colony-founding potential of previously senescent cells was stable over an extended observation period of up to 100 days (reflecting 14 serial replatings; Fig. 2b). Similar results were obtained with p53-ER^TAM as another inducible senescence gatekeeper; with γ-irradiation as an alternative senescence trigger; with ADR-exposed human lymphoma cell lines; and with colon cancer cells representing a solid, epithelial cancer type (Extended Data Fig. 3a–f). It is noteworthy that previously senescent cells typically retained the ability to re-enter TIS when re-exposed to 4-OHT and ADR, indicating that no selection for senescence-compromising mutations occurred in previously senescent cells (Extended Data Fig. 3g). Previously, an instructive, non-cell-autonomous role has been attributed to the senescence-associated secretory phenotype (SASP; reviewed in ref. 2) in models of inducible reprogramming and tissue regeneration[15,16]; however, our observations, made in pure, homotypic tumour cell populations, even under drastic reduction of SASP factor expression, favour a largely cell-intrinsic mechanism of senescence-associated reprogramming (Extended Data Fig. 4). Although we cannot completely exclude alternative explanations, these and the subsequent data strongly favour senescence-associated stemness as the most compelling and consistent interpretation of the observations presented.

Enrichment assays between matched pairs of never senescent versus previously senescent lymphomas confirmed the higher growth

competitiveness of previously senescent lymphomas both *in vitro* and *in vivo* (Extended Data Fig. 2h). Importantly, *in vivo* tumour initiation experiments found previously senescent lymphomas produced malignancies at much lower transplanted cell numbers in immune-competent recipient mice when compared to never senescent lymphomas (Fig. 2c). Taken together, the SAS program exerts its detrimental effect on tumour initiation upon release from TIS, thereby unmasking an unexpected tumour-promoting capability of the senescence program.

To test which key stemness pathways drive SAS, we used GSEA in ADR-exposed control;*Bcl2* versus *Suv39h1⁻;Bcl2* lymphomas for numerous gene sets related to Notch, Hedgehog, and canonical and non-canonical Wnt signalling. Canonical Wnt and, to some extent, Notch signalling, appeared to be significantly enriched in TIS (Extended Data Fig. 5a, b). Because Wnt signalling plays a central role in stem-cell renewal in many tissues including the haematopoietic compartment, induces Notch signalling, and is required for cancer stem cell development in haematological malignancies[18,19], we considered activation of the Wnt cascade as the putative driver behind the newly acquired stemness features in TIS lymphomas. Indeed, we detected enhanced, predominantly nuclear expression and transcriptional activation of β-catenin in control;*Bcl2* but not in *Suv39h1⁻;Bcl2* lymphomas, as well as in TIS-capable human cancer cell lines after ADR treatment (Fig. 3a, Extended Data Fig. 2b and Extended Data Fig. 5c, d). Independent of Wnt ligand–receptor stimulation, we identified inhibition of the β-catenin degradation-promoting glycogen synthase kinase 3β (GSK3β) via activated MEK–MAPK and PI3K–Akt signalling—which is
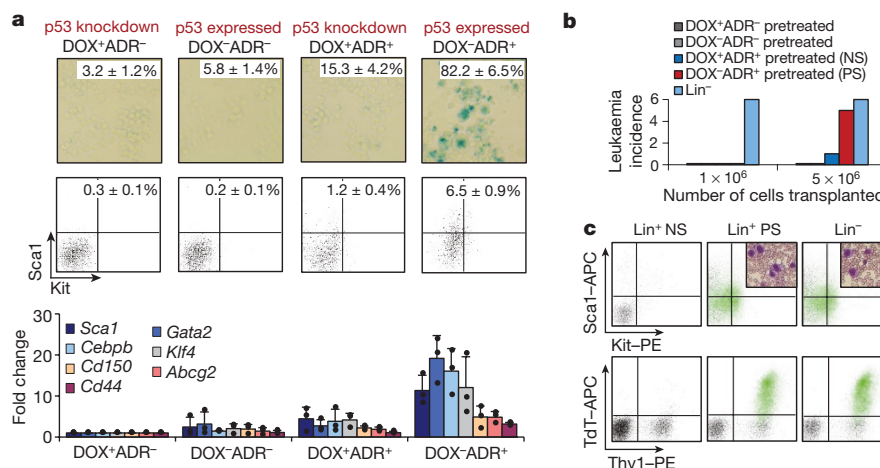
Figure 4 | Cellular senescence catalyses *de novo* reprogramming of non-stem bulk leukaemia cells into leukaemia-initiating cells. a, Stemness-related features in conditionally senescent mouse *Kras*[G12D];DOX-sh*p53*–GFP;*Bcl2* bulk leukaemia cells (Lin⁻Kit⁺Sca1⁺-depleted) treated for five days with ADR ± doxycycline (DOX)). Senescence induction is demonstrated by SA-β-gal staining (top), expression of stem-cell markers Kit and Sca1 analysed by flow cytometry (middle), and relative expression of the indicated transcripts by qPCR (bottom). Numbers reflect mean percentages of positive cells (top, middle) or average fold induction (bottom) ± s.d. (*n* = 3 biologically independent samples). **b**, Tumour initiation capacity of bulk leukaemia cells pretreated *in vitro* as in **a**, cultivated in ADR-free/DOX-supplemented medium for an additional two passages and transplanted at indicated cell numbers. Lin⁻ cells were propagated without ADR. Numbers indicate leukaemia-bearing mice out of six animals per group transplanted, within an observation period of up to 100 days (*n* = 6 mice per treatment group). **c**, Flow cytometry plots showing peripheral blood phenotyping of mice transplanted as in **b**. The GFP⁺ leukaemia cells are depicted in green. The insets show photomicrographs of peripheral blood smears stained with haematoxylin and eosin, showing leukaemic blasts (typically not detectable in never senescent recipients). One representative out of three independent experiments shown.

typically upregulated in senescence[20]—as the cell-autonomous driver of the Wnt program (Extended Data Fig. 6). The implementation of the Wnt program was further promoted by epigenetically permissive remodelling at promoters of stem-cell- and Wnt signalling-related genes in previously senescent as compared to never senescent cells (Fig. 3b). Accordingly, we found that the increased colony-forming potential of previously senescent lymphoma or colon cancer cells was dependent on Wnt signalling, as genetic or pharmacological disruption of the Wnt–β-catenin cascade—without preventing TIS or profoundly affecting cell viability—neutralized the higher clonogenicity of previously senescent cells (Fig. 3c and Extended Data Fig. 7a–d). In contrast to the never senescent cell population, a rarely dividing and strongly β-catenin-expressing subpopulation was detectable in the previously senescent cells only, and maintained at a stable steady state, explaining the lastingly enhanced colony-forming potential of previously senescent compared to never senescent cells (Extended Data Fig. 8). Consistently, the biology of the previously senescent state translated into shortened survival when previously senescent and never senescent cells were propagated in mice, whereas exposure to Wnt inhibitors *in vivo* or stable lymphoma cell transduction with a construct expressing short hairpin RNA (shRNA) against *Ctnnb1* (which encodes β-catenin) improved the poor long-term outcome of mice harbouring previously senescent lymphomas (Fig. 3d and Extended Data Fig. 7b, e, f).

Importantly, cell cycle re-entry out of TIS—as a prerequisite to exert stem-cell potential—is not limited to conditional, switchable systems, but may, as a rare event, spontaneously occur in control;*Bcl2* lymphomas, as demonstrated by the emergence of EdU-co-positive cells out of a solely SA-β-gal-positive senescent cell population (Extended Data Fig. 9). Given their stem-cell potential, we postulated that β-catenin-positive previously senescent cells might be enriched in lymphomas that progressed after chemotherapy. Hence, when comparing primary control;*Bcl2* lymphomas before therapy with the same individual lymphomas that had relapsed after exposure to senescence-inducing cyclophosphamide chemotherapy *in vivo*[8], we found a much higher fraction of cells positive for nuclear β-catenin in relapse lymphomas that also presented with higher expression levels of Wnt target genes (Fig. 3e, f, left). Moreover, longitudinally matched biopsy pairs from the same individual patients diagnosed with diffuse large B-cell lymphoma (DLBCL) before chemotherapy and at disease recurrence revealed significantly more nuclear β-catenin-positive tumour cells in the previously chemotherapy-exposed, re-emerging samples (Fig. 3f, right), further supporting a link between activated Wnt signalling in relapsed tumours and senescence-related tumour cell reprogramming. Taken together, TIS-associated stemness reflects a Wnt-governed capability that is stably maintained in a reprogrammed, hierarchically organized subpopulation of post-senescent tumour cells and critically associated with tumour progression and treatment failure.

As presumably applying to various human tumours including aggressive lymphomas, Eμ-*Myc* transgenic mouse lymphomas do not originate from a distinct fraction of cancer stem cells, because almost all lymphoma cells possess tumour-initiating potential in this model[21]. Consequently, next we asked whether cellular senescence might account for the reprogramming of non-stem tumour cells into cancer stem cells[22], in tumour types in which the tumour-initiating capacity is confined to a rare subpopulation. We isolated a non-self-renewing population of leukaemia cells from a mouse model of T-cell acute lymphoblastic leukaemia (T-ALL) driven by oncogenic *Kras*[G12D] and conditional inactivation of *p53* via a doxycycline-controlled shRNA (shp53)[23] (Extended Data Fig. 10a). ADR exposure induced senescence in the majority of non-stem leukaemia cells only if p53 expression was not cancelled (Fig. 4a, top). This group exhibited a significant conversion to Kit⁺Sca1⁺ cells, indicative of putative leukaemia stem cells (*P* = 0.02, compared to ADR-exposed but p53-deficient cells; Fig. 4a, middle), and higher expression of stem-cell-related transcripts (Fig. 4a, bottom). Upon release from TIS by knockdown of *p53*, these leukaemia cells resumed proliferation (thereby becoming previously senescent cells), and formed significantly more colonies as compared to their equally ADR-treated never senescent leukaemia counterparts that remained *p53*-inactive throughout the experiment (Extended Data Fig. 10b). As reported for TIS lymphomas, cells with nuclear β-catenin expression were almost exclusively detectable in the senescent leukaemia cell population, and Wnt inhibitors completely neutralized the increased colony formation potential of their previously senescent progeny (Extended Data Fig. 10c, d). Most importantly, almost all samples of previously senescent cells—and nearly none of the

samples of never senescent cells—initiated leukaemias in recipient mice ($P = 0.0275$, comparing previously senescent and never senescent groups); as expected, all Lin⁻ transplants gave rise to leukaemias ($P < 0.001$, comparing Lin⁻ and never senescent groups; Fig. 4b, c). Notably, and further adding to SAS in oncogene-induced senescent colon mucosa cells or melanocytes (compare with Fig. 1d), TIS reprogramming is not restricted to cells of lymphoid origin, as demonstrated for an acute myeloid leukaemia (AML) mouse model[24], culture-established human AML cells, and primary human leukaemic blast samples obtained at diagnosis from patients with AML (Extended Data Fig. 10e–l). Thus, cellular senescence is not only associated with additional stem-cell features in tumour cells with pre-existing self-renewal capability, but also catalyses the cell-autonomous reprogramming of non-stem bulk tumour cells of lymphoid and non-lymphoid origin into de novo cancer stem cells.

We present here an unexpected cell-intrinsic link between the senescence program and the acquisition of self-renewing properties, which we postulate serves as a physiological rescue mechanism in development and tissue homeostasis. We and others have observed that senescence not only occurs in critically stressed cells, but also may spread to adjacent cells via SASP components in a paracrine fashion (ref. 25; J.R.D. and C.A.S., unpublished observations). We propose that nature equipped normal cells with a latent SAS capacity (compare with Extended Data Fig. 1g) to counter the imminent loss of an entire tissue compartment due to pro-apoptotic and pro-senescent stresses: in rare cells spontaneously re-entering the cell cycle when threatening stresses no longer apply, SAS may become a tissue-replenishing principle. In a neoplastic context, cellular senescence—particularly in tumour cells with apoptotic defects—appears to be primarily a beneficial response by keeping tumour growth in check. However, post-senescent cells with 'hijacked' SAS exert their detrimental potential at relapse by driving a much more aggressive growth phenotype. Therefore, pharmacological strategies to specifically eliminate senescent cells before a fraction of them may implement their acquired stemness capacity become, as previously reported by us regarding cancer[9] and by others regarding ageing-related pathologies[26,27], a critical therapeutic need.

Online Content Methods, along with any additional Extended Data display items and Source Data, are available in the online version of the paper; references unique to these sections appear only in the online paper.

1. Muñoz-Espín, D. & Serrano, M. Cellular senescence: from physiology to pathology. *Nat. Rev. Mol. Cell Biol.* **15,** 482–496 (2014).
2. Pérez-Mancera, P. A., Young, A. R. & Narita, M. Inside and out: the activities of senescence in cancer. *Nat. Rev. Cancer* **14,** 547–558 (2014).
3. Zon, L. I. Intrinsic and extrinsic control of haematopoietic stem-cell self-renewal. *Nature* **453,** 306–313 (2008).
4. Krizhanovsky, V. *et al.* Implications of cellular senescence in tissue damage response, tumor suppression, and stem cell biology. *Cold Spring Harb. Symp. Quant. Biol.* **73,** 513–522 (2008).
5. Serrano, M., Lin, A. W., McCurrach, M. E., Beach, D. & Lowe, S. W. Oncogenic *ras* provokes premature cell senescence associated with accumulation of p53 and p16^INK4a. *Cell* **88,** 593–602 (1997).
6. Braig, M. *et al.* Oncogene-induced senescence as an initial barrier in lymphoma development. *Nature* **436,** 660–665 (2005).
7. Michaloglou, C. *et al.* BRAF^E600-associated senescence-like cell cycle arrest of human naevi. *Nature* **436,** 720–724 (2005).
8. Schmitt, C. A. *et al.* A senescence program controlled by p53 and p16^INK4a contributes to the outcome of cancer therapy. *Cell* **109,** 335–346 (2002).
9. Dörr, J. R. *et al.* Synthetic lethal metabolic targeting of cellular senescence in cancer therapy. *Nature* **501,** 421–425 (2013).
10. Onder, T. T. *et al.* Chromatin-modifying enzymes as modulators of reprogramming. *Nature* **483,** 598–602 (2012).
11. Krizhanovsky, V. & Lowe, S. W. Stem cells: The promises and perils of p53. *Nature* **460,** 1085–1086 (2009).
12. Rea, S. *et al.* Regulation of chromatin structure by site-specific histone H3 methyltransferases. *Nature* **406,** 593–599 (2000).
13. Narita, M. *et al.* Rb-mediated heterochromatin formation and silencing of E2F target genes during cellular senescence. *Cell* **113,** 703–716 (2003).
14. Chen, J. *et al.* H3K9 methylation is a barrier during somatic cell reprogramming into iPSCs. *Nat. Genet.* **45,** 34–42 (2013).
15. Mosteiro, L. *et al.* Tissue damage and senescence provide critical signals for cellular reprogramming *in vivo*. *Science* **354,** aaf4445 (2016).
16. Ritschka, B. *et al.* The senescence-associated secretory phenotype induces cellular plasticity and tissue regeneration. *Genes Dev.* **31,** 172–183 (2017).
17. Wong, D. J. *et al.* Module map of stem cell genes guides creation of epithelial cancer stem cells. *Cell Stem Cell* **2,** 333–344 (2008).
18. Reya, T. *et al.* A role for Wnt signalling in self-renewal of haematopoietic stem cells. *Nature* **423,** 409–414 (2003).
19. Wang, Y. *et al.* The Wnt/beta-catenin pathway is required for the development of leukemia stem cells in AML. *Science* **327,** 1650–1653 (2010).
20. Lin, A. W. *et al.* Premature senescence involving p53 and p16 is activated in response to constitutive MEK/MAPK mitogenic signaling. *Genes Dev.* **12,** 3008–3019 (1998).
21. Kelly, P. N., Dakic, A., Adams, J. M., Nutt, S. L. & Strasser, A. Tumor growth need not be driven by rare cancer stem cells. *Science* **317,** 337 (2007).
22. Chaffer, C. L. *et al.* Normal and neoplastic nonstem cells can spontaneously convert to a stem-like state. *Proc. Natl Acad. Sci. USA* **108,** 7950–7955 (2011).
23. Zhao, Z. *et al.* p53 loss promotes acute myeloid leukemia by enabling aberrant self-renewal. *Genes Dev.* **24,** 1389–1402 (2010).
24. Zuber, J. *et al.* RNAi screen identifies Brd4 as a therapeutic target in acute myeloid leukaemia. *Nature* **478,** 524–528 (2011).
25. Acosta, J. C. *et al.* A complex secretory program orchestrated by the inflammasome controls paracrine senescence. *Nat. Cell Biol.* **15,** 978–990 (2013).
26. Baker, D. J. *et al.* Naturally occurring p16^Ink4a-positive cells shorten healthy lifespan. *Nature* **530,** 184–189 (2016).
27. Baar, M. P. *et al.* Targeted apoptosis of senescent cells restores tissue homeostasis in response to chemotoxicity and aging. *Cell* **169,** 132–147.e16 (2017).
28. Pawlikowski, J. S. *et al.* Wnt signaling potentiates nevogenesis. *Proc. Natl Acad. Sci. USA* **110,** 16009–16014 (2013).
29. Haugstetter, A. M. *et al.* Cellular senescence predicts treatment outcome in metastasised colorectal cancer. *Br. J. Cancer* **103,** 505–509 (2010).

Author Contributions M.Mi. performed mouse lymphoma and leukaemia work, stem-cell and senescence assays, and gene set enrichment analyses. J.H.M.D. and M.R. conducted analyses with human cancer cell lines and primary human material. D.N.Y.F. and D.B. carried out flow cytometric analyses. Z.Z. generated leukaemias in the p53-regulatable mouse T-ALL model, I.A.M.B. and J.Z. in the p53-regulatable mouse AML model. Y.Y. carried out biochemical analyses. J.R.D. provided transcriptome analyses and long-term outcome data from senescence-capable mouse lymphomas. L.D. and M.A.M.-P. performed chromatin immunoprecipitations and analysed related datasets. D.L. conducted Affymetrix gene expression profiling and analyses. T.K. and G.D. carried out proteome analyses. M.Me. generated β-catenin/TCF-reporter cancer cell lines and performed luciferase reporter assays. K.P. generated qPCR data. A.T., B.D., H.G. and S.L. contributed to study design, data interpretation and preparation of the manuscript. M.H. provided immunohistochemical analyses. C.A.S. designed experiments, analysed the data and wrote the manuscript.

METHODS

Generation of primary mouse lymphomas and leukaemias, and use of primary human B-cell lymphoma, B-CLL and AML samples. All animal protocols used in this study were approved by the governmental review board (Landesamt Berlin), and conform to the respective regulatory standards. Lymphomas with defined genetic defects were generated by intercrossing Eμ-*Myc* transgenic mice to mice carrying loss-of-function alleles at the *Suv39h1* locus[30,31] or to mice harbouring a 4-OHT-inducible *p53-ER*[TAM] knock-in allele, encoding a p53–oestrogen receptor fusion protein that is inactive in the absence of 4-OHT[32], all in a C57BL/6 background. Eμ-*Myc* transgenic lymphomas that formed in Eμ-*Myc*;*p53-ER*[Tam/+] mice with an allelic loss of the remaining *p53* wild-type allele were designated *p53-ER*[Tam] lymphomas. *Suv39h1*^{−/−} lymphomas reflect Eμ-*Myc* lymphomas that arose in *Suv39h1*^{−/−} females or, owing to the X-linkage of the *Suv39h1* locus, in *Suv39h1*[Y/−] males[33]. Genotyping of the offspring by allele-specific genomic PCR, monitoring of lymphoma onset and isolation of viable lymphoma cells were carried out as described[8,34]. *Kras*[G12D];shp53-GFP-induced T-cell acute lymphoblastic leukaemias (T-ALL) with tetracycline (that is, doxycycline)-dependent shp53 expression ('DOX-on') were generated and isolated following a previously published protocol with minor modifications[23,35]. The *Nras*[G12D]/MLL-AF9-driven mouse model of acute myeloid leukaemia (AML), co-expressing a reverse tetracycline transactivator ('Tet-on competent'), was generated as previously described[24]. Six- to eight-week-old C57BL/6 ('wild type') female mice were used as recipients for *in vivo* lymphoma or leukaemia propagation. No randomization or blinding was used to allocate experimental groups.

The use of tumour biopsies (that is, bone marrow aspirates, lymph-node biopsies or peripheral blood samples obtained for the initial diagnosis or follow-up analyses of patients with B-cell leukaemia (B-CLL), diffuse large B-cell lymphoma (DLBCL) or acute myeloid leukaemia (AML)) as anonymous samples after informed patient consent was approved by the local ethics commission of the Charité – Universitätsmedizin Berlin (reference EA4/085/07 and EA4/061/11).

Cell culture, plasmids and retroviral gene transfer. Isolated mouse lymphoma cells and primary human AML samples (tumour-cell-purified by Ficoll density-gradient centrifugation and red cell lysis) were short-term cultured in standard medium on irradiated NIH3T3 fibroblast feeders[36]. Primary human B-cell malignancies were cultivated in a 'CD40 system'[37], that is, in the same medium further supplemented with 100 IU ml^{−1} of recombinant human interleukin-4 (Peprotech) on irradiated NIH3T3 cells stably expressing the human CD40 ligand. Human cancer cell lines were obtained from DSMZ (Leibniz-Institut Deutsche Sammlung von Mikroorganismen und Zellkulturen GmbH), ATCC or Biomol: RCK8 (DSMZ; ACC-561), Eheb (DSMZ; ACC-67), K562 (DSMZ; ACC-10), Mec1 (DSMZ; ACC-497), Molm13 (DSMZ; ACC-554), SW480 (DSMZ; ACC-313), LS174T (DSMZ; ACC-759), DLD-1 (DSMZ; ACC-278), Caco-2 (DSMZ; ACC-169), SKMel28 (ATCC; HTB-72), MeWo (ATCC; HTB-65), WM266.4 (Biomol; WM266-4-01). Omm2.3 cells were provided by Martina J. Jager. The cells were cultivated according to the supplier's recommendations and regularly tested for mycoplasma contamination. The cell lines bought within last four years were not additionally authenticated (RCK8, Eheb, Mec-1). All other cell lines were authenticated by DSMZ using a single-nucleotide polymorphism-based multiplex approach in October 2017. Single-nucleotide polymorphism profiles matched known profiles or were unique (Omm2.3). Retroviral supernatants, generated by transient transfection of Phoenix-Eco packaging cells with murine stem-cell retrovirus (MSCV)-based constructs, were used to stably infect Eμ-*Myc* transgenic lymphomas, *Kras*[G12D];shp53–GFP T-ALL cells, *Nras*[G12D]/MLL-AF9 AML cells or human cancer cell lines (engineered to express the ecotropic virus receptor as described[38]). Freshly isolated cells were first infected with an MSCV retrovirus encoding murine or human *Bcl2* and a blasticidin antibiotic resistance gene. *Bcl2*-overexpressing Eμ-*Myc*;*Suv39h1*[−] lymphoma were subsequently infected with *Suv39h1-ER*[T2] cDNA, encoding murine full-length *Suv39h1,* fused in frame with the coding sequence of an 4-OHT-inducible oestrogen receptor mutant (ER[T2]; see ref. 39), subcloned into MSCV-IRES–GFP or MSCV-IRES-DsRed vectors. GFP- or DsRed-positive cells were purified in a fluorescence-activated cell sorter (FACS Aria II, BD Biosciences). TOPflash and FOPflash reporter constructs (reflecting the wild-type or mutant TCF-binding promoter region followed by a firefly luciferase-encoding cDNA) were subcloned from the original pGL3 vector into a self-inactivating MSCV[SIN]-DsRed plasmid, stably transferred into mouse lymphoma cells or human cell lines (expressing the ecotropic virus receptor), and flow-sorted for DsRed-positive cells. NF-κB inactivation was achieved by stable overexpression of an IκBαΔN construct (NF-κB super-repressor (NF-κB-SR)) in control;*Bcl2* cells as reported previously[40]. Wnt pathway activation was achieved by transducing control;*Bcl2* lymphomas with a stabilized murine β-catenin (encompassing an N-terminal 90-amino acid deletion, [ΔN]β-catenin)-encoding MSCV-IRES–GFP retrovirus. To stably knock down *β-catenin* expression, a previously published shRNA sequence[41] was subcloned into the pSuperRetro plasmid to infect

Suv39h1[−];*Bcl2*;*Suv39h1*-ER[T2] cells. An MSCV[SIN]-based construct containing a miR30-shRNA against murine *p53* under a tetracycline-dependent promoter[42] was used to transfect *Nras*[G12D]/MLL-AF9;*Bcl2* cells. Stable *TP53* knockdown in human cell lines RCK8, Molm-13 and LT174T was achieved by lentiviral transduction with a previously published shRNA against *p53* (ref. 43) in the pLKO.1-puro vector (Addgene plasmid 19119).

In vitro and in vivo treatments. For the induction of cellular senescence *in vitro*, Adriamycin (ADR; Sigma), a topoisomerase II inhibitor widely used in the clinic to treat lymphomas and other malignancies, was added once at a concentration of 0.05 μg ml^{−1} in all experiments, with the following exceptions: Eheb, Mec1, Molm13 and RCK8 cell lines, treated with 0.01 μg ml^{−1} ADR, and the K562 cell line, treated with 0.025 μg ml^{−1} ADR. For conditional activation of ER[Tam]- or ER[T2]-fused constructs, the cells were additionally exposed over five days to 1 μM of 4-OHT (Sigma) or the equivalent volume of the ethanol-based solvent. Cellular senescence was assessed after five days of treatment. Pharmacological inhibition of the Wnt pathway or kinases involved in modulating Wnt signalling was performed by adding small molecule inhibitors to the cells for the final 48 h of the senescence-inducing ADR ± 4-OHT treatment: Wnt inhibitors ICG-001 (10 μM; Enzo Life Sciences) and salinomycin (1 μM; Sigma), MAPK inhibitor PD325901 (10 nM; Selleckchem), MEK inhibitor PD98059 (25 μM; Selleckchem), PI3K inhibitor LY294002 (10 μM, Sigma-Aldrich), Akt inhibitor MK-2206 (200 nM, Selleckchem) or GSK3β inhibitor CHIR99021 (1 μM; Sigma-Aldrich). For Wnt-modulating treatments upon senescence-release, passage-2 never senescent and previously senescent cells were used (that is, ADR ± 4-OHT-pretreated Eμ-*Myc*; *Suv39h1*[−];*Bcl2*;*Suv39h1*-ER[T2] cells, further propagated in 4-OHT/ADR-free medium for 14 days). Matched pairs of previously senescent and never senescent cells were exposed to Wnt inhibitors as described above, or to recombinant mouse Wnt3a (10 ng ml^{−1}, R&D Systems), recombinant mouse R-Spondin 2 (Rspo2; 20 ng ml^{−1}, R&D Systems), a combination of the two ligands (at the same concentration as for single ligands) or to the GSK3β inhibitor CHIR99021 (1 μM, Sigma-Aldrich) for 48 h regarding the gene expression analysis or for seven days (in methylcellulose medium) regarding colony formation assessment. The doxycycline (DOX)-dependent activation of an shRNA against *p53* in mouse *Kras*[G12D];shp53–GFP T-ALL or *Nras*[G12D]/MLL-AF9 AML samples was achieved by supplementing the culture medium with 1 μg ml^{−1} of doxycycline (Sigma).

For *in vivo* experiments, 1×10^6 Eμ-*Myc*;*Suv39h1*[−];*Bcl2*;*Suv39h1*-ER[T2] lymphoma or 5×10^6 *Kras*[G12D];shp53–GFP T-ALL leukaemia cells (or 1×10^6 Lineage[−] (Lin^{−}) cells as a positive control), if not otherwise indicated, were transplanted by tail-vein injection into immunocompetent recipient mice. In case of *Kras*[G12D];shp53–GFP T-ALL leukaemia samples, recipient mice were irradiated with 6 Gy, 24 h before transplantation. DOX was supplied with the drinking water (20 mg ml^{−1}; exchanged twice a week) and in food pellets (200 mg kg^{−1} of regular chow). Leukaemia manifestation was diagnosed by flow cytometry-based detection of GFP-positive cells in the peripheral blood at the time mice presented with general signs of pre-terminal sickness (greater than 20% weight loss or other symptoms of severe sickness). If no signs of sickness were noted, the experiments were ended by 70% tumour burden in peripheral blood. Lymphoma formation was diagnosed when palpable lymph-node enlargements had formed. A tumour size of 16 mm (corresponding to approximately 4 lymph nodes of 4 mm in diameter) was approved by Landesamt Berlin as an experiment end-point criterion and was not exceeded in any of the performed experiments. ICG-001 and salinomycin were applied intraperitoneally daily (both at a dose of 10 mg kg^{−1} body weight), starting from palpable lymphoma formation until a pre-terminal disease stage was reached. Time-to-death was defined as the latency between transplantation and a pre-terminal disease stage. Upon CO_2 euthanasia, single-cell suspensions were isolated from enlarged organs as described previously[8,36].

Analysis of growth parameters, viability, stem-cell and senescence markers. Cell-cycle analysis by 5-bromo-2′-deoxyuridine/propidium iodide (BrdU/PI)-based flow cytometric measurement was performed as described previously[33]. Cytospin preparations of suspension cultures for subsequent SA-β-gal analyses or immunostainings were carried out as described previously[6,44,45]. Carboxyfluorescein succinimidyl ester (CFSE) labelling was performed on day 3 after starting ADR ± 4-OHT treatment, using the CellTrace Far Red Cell Proliferation Kit for flow cytometry (Molecular Probes, C34564) according to the manufacturer's recommendations. CFSE^{high} cells were sorted on treatment day 5 on an S3e Cell Sorter (Bio-Rad). For β-catenin co-staining, CFSE-labelled cells were fixed in 4% paraformaldehyde, permeabilized by Saponin in 1% bovine serum albumin (LifeTechnologies, 10635), stained with Alexa Fluor 488 mouse anti-β-catenin antibody according to the manufacturer's recommendations (BD Pharmingen, 562505), and acquired on an ImageStreamX Mark II Imaging Flow Cytometer (Amnis, MerckMillipore). EdU labelling was performed on treatment day 5 using the Click-iT EdU Pacific Blue Flow Cytometry Assay Kit according to the manufacturer's recommendations (Molecular Probes, C10418). For the fluorescent SA-β-gal labelling, cells

were incubated in 75 μM chloroquine solution for 1 h followed by exposure to the C12FDG substrate (5-dodecanoylaminofluorescein-di-β-D-galactopyranoside; ImaGene Green C12FDG *lacZ* Gene Expression Kit, Molecular Probes, I2904) for 20 min at 37 °C in PBS (pH 5.5, with 1 mM MgCl₂) and analysed on ImageStreamX Mark II Imaging Flow Cytometer. Cell viability was evaluated by annexin V (BD Pharmingen, 556419) and propidium iodide (5 μg ml⁻¹, Sigma-Aldrich) staining, analysed in a FACSCalibur flow cytometer (BD Biosciences). Viable cells were detected as annexin V/propidium iodide-double-negative. ABC transporter activity was analysed using the eFluxx-ID Gold multidrug resistance kit (Enzo Life Sciences), and ALDH activity using the ALDEFLUOR kit (StemCell Technologies)[46], according to the manufacturer's instructions. Colony-forming unit assays were performed by plating 10^2 or 10^3 cells in 1 ml of methylcellulose medium (MethoCult M3134 for mouse cells, or H4100 for human cells, Stem Cell Technologies). For mouse cells, the medium was supplemented with recombinant murine interleukin (IL)-3 (1 ng ml⁻¹, Miltenyi), recombinant murine IL-6 (10 ng ml⁻¹, Miltenyi), recombinant murine IL-7 (0.1 ng ml⁻¹, Peprotech), and recombinant murine stem-cell factor (SCF, 50 ng ml⁻¹, Peprotech). For the indicated assays, the medium was further supplemented with ADR (0.05 μg ml⁻¹), 4-OHT (1 μM), DOX (1 μg ml⁻¹), ICG-001 (10 μM), salinomycin (1 μM)[47,48], Wnt3a (10 ng ml⁻¹), Rspo2 (20 ng ml⁻¹) or GSK3β inhibitor CHIR99021 (1 μM). Clusters of greater than 50 cells were scored as colonies, using bright-field or fluorescence microscopy. For serial passaging, cells were washed out of methylcellulose with warm PBS after seven days (mouse B-cell lymphoma cells) or ten days (mouse T-ALL cells), counted and plated in fresh methylcellulose medium (10^2 or 10^3 cells per ml). Regarding luciferase-based Wnt reporter assays, cells stably transfected with TOPflash-MSCV_SIN or FOPflash-MSCV_SIN were ADR-exposed in a senescence-inducing schedule as described above. The luminescence signals were measured with the ONE-Glo kit (Promega) according to the manufacturer's instructions and normalized to viable cell counts. For depletion of Lin⁻ cells from $Kras^{G12D}$;shp53–GFP T-ALL samples or $Nras^{G12D}$/MLL-AF9 AML samples, cells were labelled with a cocktail of biotinylated lineage marker antibodies (BD Biosciences, 559971) followed by Streptavidin-PE (BD Biosciences, 554061). GFP⁺PE⁺ cells were flow-sorted in a FACS Aria II (BD Biosciences). For depletion of CD34⁺ cells from *Bcl2*-transfected Molm-13 cell line, cells were stained with a directly conjugated anti-CD34-APC antibody (1:200, BD Biosciences, 560940), and CD34⁻ cells were sorted in a FACS Aria II (BD Biosciences).

RNA-based expression analysis. For microarray-based gene expression profiling of untreated or five-day-ADR-exposed control;*Bcl2* or *Suv39h1⁻*;*Bcl2* lymphomas, RNA was isolated and processed as previously reported[40].

The list of 5,401 probe sets differentially expressed between untreated and ADR-treated control;*Bcl2* lymphomas was determined by analysis of variance (ANOVA, cut-off at $q < 0.05$). The list of filtered genes was ranked according to expression fold changes, and the genes belonging to the ATSC[17] or core embryonic stem-cell signature[49] were marked in orange and blue, respectively.

Gene set enrichment analysis (GSEA) was performed with the GSEA v2.0 software (Broad Institute of MIT (Massachusetts Institute of Technology) and Harvard, http://www.broad.mit.edu/gsea)[50] on transcriptome data produced in our laboratory (GSE31099 and GSE44355) or on publicly available transcriptome datasets downloaded from the Gene Expression Omnibus (GEO; https://www.ncbi.nlm.nih.gov/geo/): normal colon epithelium and colon adenomas from $Apc^{Min/+}$ mice (GSE422, samples GSM6191–GSM6201), Braf-V600E-infected human melanocytes (GSE46801), human mammary epithelial cells in p16^INK4a-dependent stasis or telomere shortening-induced agonescence (GSE16058), normal human foreskin BJ fibroblasts in replicative senescence (GSE13330, samples GSM336385–GSM336628) and normal human mesenchymal stem cells in replicative senescence (GSE9593, samples GSM242185, GSM242668, GSM242669 and GSM242672–GSM242674). Probed gene sets were taken without further change from the indicated publications, downloaded from the Molecular Signature Database (MsigDB) of the Broad Institute (http://software.broadinstitute.org/gsea/msigdb/collections.jsp) or from the Gene Ontology (GO) browser AmiGO ('GO Cell cycle process' (GO:0022402), GO 'Wnt signaling pathway' (GO0016055), GO 'Canonical Wnt receptor signaling' (GO:0060070), GO 'Noncanonical Wnt signaling' (GO0035567), GO 'Notch signaling pathway' (GO0007219), GO 'Smoothened signaling pathway' (GO0007224)), or generated from the gene list reflecting the Mouse Wnt Signalling Pathway PCR Array (SA Biosciences; genes from this list annotated to have a role in cell growth and proliferation were used as a separate gene set, http://www.sabiosciences.com/rt_pcr_product/HTML/PAMM-043A.html#function). Normalized enrichment scores (NES) with P values <0.05 and false discovery rates (FDR) <0.25 were considered statistically significant.

For quantitative reverse-transcriptase PCR analyses of stem-cell-related genes in lymphoma cells, RNA extracted with Trizol (Invitrogen) was transcribed into cDNA using SuperScript II reverse transcriptase (Invitrogen). A panel of established stem-cell-related markers consisting of mouse *Abcg2*, *Cebpb*, *Kit*, *Cd34*, *Cd44*, *Prom1* (also known as *Cd133*), *Slamf1* (also known as *Cd150*), *Klf4*, *Ly6a* (also known as *Sca1*) or human *ABCG2*, *CD34*, *CD44*, *PROM1* (also known as *CD133*), *SLAMF1* (also known as *CD150*), *LGR5*, a panel of Wnt signalling targets: *Ccnd1*, *Fosl1*, *Fzd3*, *Id2*, *Met*, as well as a panel of established mouse SASP factors: *Igfbp6*, *Ccl2*, *Ccl20*, *Cxcl1*, *Ctgf*, *Il6*, *Kitl* and *Tnfa* were analysed by qPCR using commercially available Taqman assays (Applied Biosystems). Transcript quantification was calculated as $2^{(-\Delta Ct)}$ based on $\Delta C_t = \Delta C_{t(treated)} - \Delta C_{t(untreated)}$, with *GAPDH* transcript levels as an internal control.

Protein-based expression analyses. Immunophenotyping by flow cytometry was carried out as described previously[8,45], using the primary antibodies directed against human CD34 (BD Biosciences, 560940, 1:200), human CD33 (BD Biosciences, 555450 1:200), or against mouse antigens: H3K9me3 (Abcam, ab8898, 1:2,000), β-catenin (eBiosciences, 50-2567, 1:20), Thy1.2 (BD Biosciences, 553005, 1:200), TdT (Miltenyi, 130-100-749, 1:10), Kit (BD Biosciences, 553355, 1:200), Sca1 (BD Biosciences, 557404, 1:200), followed by secondary antibodies: anti-rabbit AlexaFluor 594 (Invitrogen A21207, 1:200) and Streptavidin-APC (BD Biosciences, 554067, 1:2,000).

For immunoblotting analyses, whole-cell pellets were lysed in Laemmli sample buffer (60 mM Tris-HCl at pH 6.8, 10% glycerol, 2% SDS, 5% 2-mercaptoethanol) supplemented with protease and phosphatase inhibitors, resolved by electrophoresis on a 12% SDS polyacrylamide gel (SDS–PAGE), transferred onto an Immobilon-P membrane (Millipore) and probed using antibodies against total β-catenin (BD Biosciences, 610153, 1:200), active β-catenin (dephosphorylated at serine 37 (Ser37) and threonine 41 (Thr41); Millipore, 05-665, 1:1,000), H3K9me3 (Abcam, ab8898, 1:2,000), total Erk (Cell Signaling Technology (CST), 9102, 1:1,000), phospho-Erk1/2 (that is, Erk1/2 phosphorylated at Thr202 and Tyr204; CST, 4376, 1:1,000), total Akt (CST, 9272, 1:1,000), phospho-Akt (that is, Akt-P-Ser473; CST, 4060, 1:2,000), total GSK3β (CST, 12456, 1:1,000), phospho-GSK3β (that is, GSK3β-P-Ser9; CST, 5558, 1:1,000) and α-tubulin (Sigma, T5168, 1:500) as a loading control.

For immunofluorescence, cells were fixed in 4% paraformaldehyde, permeabilized with 0.1% Triton X-100/PBS, blocked in 1% bovine serum albumin supplemented with the anti-mouse Cd32/Cd16 antibody (BD Biosciences, 53142, 1:50) and incubated with a primary antibody against total β-catenin (1:200), followed by 0.01% Tween 20 as detergent buffer and Alexa Fluor 594 (Invitrogen A11008, 1:5,000) as a secondary anti-mouse IgG antibody. The slides were stained with 4,6-diamidino-2-phenylindole (DAPI, Biolegend, 422801, 1:1,000 in PBS) as a nuclear counterstain, and mounted with Mowiol 4-88 (Calbiochem). Immunohistochemistry was performed on formalin-fixed, paraffin-embedded lymph-node sections as described previously[33]. Cryo-sections of mouse lymph-nodes were stained with an fluorescein isothiocyanate-conjugated antibody against total β-catenin (BD Biosciences, 562505, 1:200), and human DLBCL sections were stained with a primary antibody against total β-catenin (BD Biosciences, 610153, 1:200), followed by a secondary anti-mouse IgG antibody (1:1,000, Dako REAL Detection System (labelled streptavidin–biotin), Dako, K5005).

Global proteome analysis. $Suv39h1⁻$;*Bcl2*;$Suv39h1$-ER^{T2} cells were sampled in ice-cold methanol after five days of ADR ± 4-OHT treatment. 50 μg of the protein extracts were digested using an xt-PAL (CTC Analytics) pipetting robot with the Chronos software package (Axel Semrau), reduced with 1 mM tris(2-carboxyethyl) phosphine. Free sulfhydryl groups were carbamidomethylated with 5.5 mM choloroacetamide. The proteins were digested using 0.5 μg sequencing-grade endopeptidase LysC (Wako) for 3 h at room temperature, and subsequently diluted with four volumes of 50 mM ammonium bicarbonate. Tryptic digestion occurred over 10 h at room temperature using 1 μg of sequencing-grade trypsin (Promega). The reaction was stopped by adding trifluoroacetic acid to a final pH of 2. The peptides were purified using C18-stage tips (3M)[51]. By applying the dimethyl labelling technique, the untreated lymphoma samples, serving as the reference, were 'light'-labelled, whereas others (ADR ± 4-OHT-treated) were 'heavy'-labelled, on the xt-PAL machine by automatically adding 4 μl light (+28 Da) or heavy (+32 Da) formaldehyde and 4 μl cyanoborohydride to a final concentration of 0.8%[52]. The reaction was carried out overnight, quenched by 16 μl of 50 mM ammonium bicarbonate buffer and acidified by 8 μl 50% trifluoroacetic acid. The 'heavy'- and 'light'-labelled samples were mixed in a 1:1 ratio and measured as technical duplicates on a Q-Exactive mass spectrometer (Thermo Fisher) coupled to a Proxeon nano-LC system (Thermo Fisher) in data-dependent acquisition mode, selecting the top ten peaks for higher-energy collisional dissociation fragmentation. A three-hour gradient (solvent A: 5% acetonitrile, 0.1% formic acid; solvent B: 80% acetonitrile, 0.1% formic acid) was applied to the samples using a custom-made nano-LC column (0.075 mm × 250 mm, 3 μm Reprosil C18, Dr. Maisch GmbH). The peptides were eluted in gradients of 4 to 76% acetonitrile and 0.1% formic acid in water at flow rates of 0.25 μl min⁻¹. Mass spectrometric acquisition was performed at a resolution of 70,000 in the scan range of 300 to 1,700 m/z. Dynamic exclusion was set to 30 s and the normalized collision energy to 26 eV. For the automatic interpre-

tation of the recorded spectral data, the MaxQuant software version 1.2.2.5 (Max Planck Institute) was used, with a multiplicity of 2 for dimethyl labelling[53]. An FDR of 0.01 was applied on the peptide and the protein level, and an Andromeda-based search was performed using a mouse International Protein Index database (ipi.MOUSE.v3.84.fasta). Mass spectrometric measurement data were log-transformed regarding the heavy/light ratios using the R-statistical software (R Foundation for Statistical Computing). Three replicates were used to calculate mean values and significance levels using the Wilcoxon test. All identifications with a $-\log_{10}$-transformed P value >1 were considered significant.
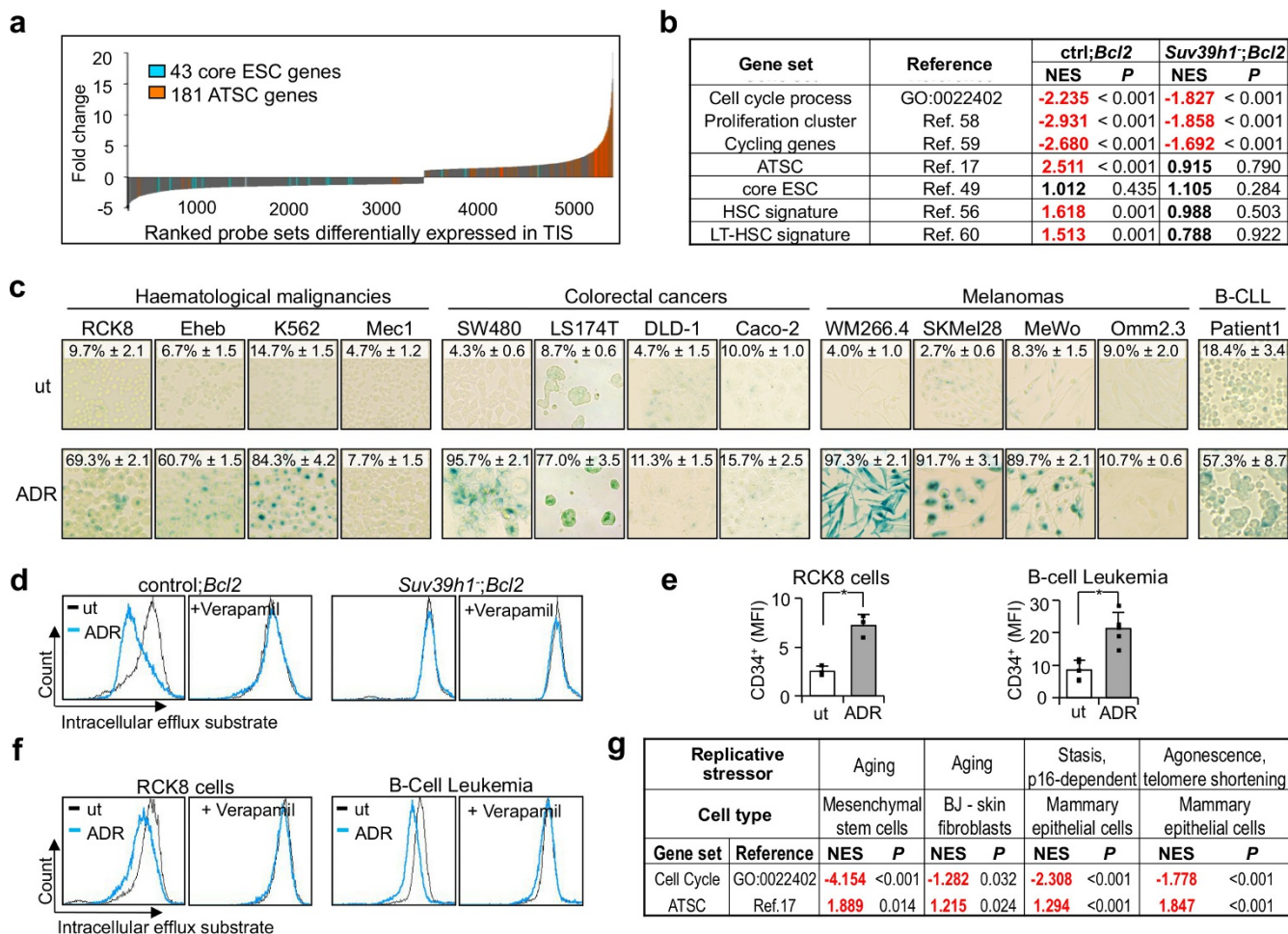
Chromatin immunoprecipitation. Chromatin immunoprecipitation was performed according to Young and colleagues[54] with minor modifications. 1×10^7 cells were fixed for 20 min in a 1% formaldehyde solution. The fixation was stopped with 0.1 M glycine, the cell pellet was lysed and sonicated in 300 μl buffer LB3[54] (Bioruptor Sonicator, two cycles of 15 min each at high power in pulsed mode (30 s on, 30 s off)). 30 μl of 10% Triton X-100 was added and the sample was centrifuged at 13,000 rpm for 10 min at 4 °C. The supernatant was removed and an aliquot was retained as the input DNA sample. For immunoprecipitation, 140 μl of the supernatant was mixed with 50 μl of Dynabeads Protein G (Life Technologies/Invitrogen), pre-coated with 5 μg of an H3K4me3 antibody (A5051-001P, Diagenode) or an H3K27me3 antibody (39155, Active Motif) and incubated at 4 °C overnight. After incubation, the beads were magnetically separated from the supernatant, washed and eluted. After reverse-crosslinking, RNaseA and proteinase K digestion[54], the DNA was extracted with phenol/chloroform, and used as a template for qPCR. Sequence information of the specific primers used is available upon request. Enrichments were calculated according to the $\Delta\Delta C_t$ method, with Prame as endogenous control, and the input as calibrator. The values of the relative enrichments for the 4-OHT/ADR-treated samples were divided by the corresponding ADR sample values.

Statistical evaluation. On the basis of previous experience with the Eμ-*Myc* transgenic mouse lymphoma model, sample sizes typically reflect three to five individual primary tumours as independent biological replicates. All quantifications from staining reactions (for example, immunostainings or SA-β-gal assays) reflect at least three samples with at least 100 events counted (typically in three different areas) each. For assessing long-term outcome after *in vivo* treatments, six or more tumour-bearing animals per arm were used. No statistical method was used to pre-determine sample size. No data were excluded, all probes/animals that met proper experimental conditions were included in the analysis. For purposes of tumour-initiation assays, a transplanted mouse scored positive if a palpable lymphadenopathy developed at any time point during the observation period of 100 days. The tumour initiation data were analysed using the ELDA (Extreme Limiting Dilution Analysis) software package at http://bioinf.wehi.edu.au/software/elda/ (ref. 55) with a confidence interval of 95%. Unless stated otherwise, data are presented as arithmetic means ± standard deviation (s.d.) and statistical analyses were based on paired or unpaired two-sided *t*-tests. The data not following a normal distribution (by Kolmogorov–Smirnov test) were analysed by unpaired *t*-test with Welch's correction. Similar variance between groups was not assumed. $P < 0.05$ was considered statistically significant. The whisker plot boxes indicate the first and third quartiles with median, and the upper and lower bars minimum and maximum values. For GSEA, the non-parametric Kolmogorov–Smirnov test was applied. Significant enrichment was accepted when $P < 0.05$ and FDR < 0.25, thus using the default significance levels for the method.

Data availability. Microarray datasets produced in our laboratory and analysed in this study are available at the Gene Expression Omnibus (GEO) repository of the National Center for Biotechnology Information, under the accession numbers GSE31099 and GSE44355, for control;*Bcl2* and *Suv39h1⁻*;*Bcl2* lymphomas, respectively. Source Data for Figs 1–4 and Extended Data Figs 1–10 are provided with the online version of this paper. All other datasets generated during this study are available from the corresponding author on reasonable request.

30. Adams, J. M. *et al.* The c-*myc* oncogene driven by immunoglobulin enhancers induces lymphoid malignancy in transgenic mice. *Nature* **318,** 533–538 (1985).
31. Peters, A. H. *et al.* Loss of the *Suv39h* histone methyltransferases impairs mammalian heterochromatin and genome stability. *Cell* **107,** 323–337 (2001).
32. Martins, C. P., Brown-Swigart, L. & Evan, G. I. Modeling the therapeutic efficacy of p53 restoration in tumors. *Cell* **127,** 1323–1334 (2006).
33. Reimann, M. *et al.* Tumor stroma-derived TGF-β limits myc-driven lymphomagenesis via Suv39h1-dependent senescence. *Cancer Cell* **17,** 262–272 (2010).
34. Schmitt, C. A. *et al.* Dissecting p53 tumor suppressor functions *in vivo*. *Cancer Cell* **1,** 289–298 (2002).
35. Premsrirut, P. K. *et al.* A rapid and scalable system for studying gene function in mice using conditional RNA interference. *Cell* **145,** 145–158 (2011).
36. Schmitt, C. A., McCurrach, M. E., de Stanchina, E., Wallace-Brodeur, R. R. & Lowe, S. W. *INK4a/ARF* mutations accelerate lymphomagenesis and promote chemoresistance by disabling p53. *Genes Dev.* **13,** 2670–2677 (1999).
37. Banchereau, J., de Paoli, P., Vallé, A., Garcia, E. & Rousset, F. Long-term human B cell lines dependent on interleukin-4 and antibody to CD40. *Science* **251,** 70–72 (1991).
38. Schmitt, C. A., Rosenthal, C. T. & Lowe, S. W. Genetic analysis of chemoresistance in primary murine lymphomas. *Nat. Med.* **6,** 1029–1035 (2000).
39. Feil, R., Wagner, J., Metzger, D. & Chambon, P. Regulation of Cre recombinase activity by mutated estrogen receptor ligand-binding domains. *Biochem. Biophys. Res. Commun.* **237,** 752–757 (1997).
40. Jing, H. *et al.* Opposing roles of NF-κB in anti-cancer treatment outcome unveiled by cross-species investigations. *Genes Dev.* **25,** 2137–2146 (2011).
41. Yang, D. H. *et al.* Wnt5a is required for endothelial differentiation of embryonic stem cells and vascularization via pathways involving both Wnt/β-catenin and protein kinase Cα. *Circ. Res.* **104,** 372–379 (2009).
42. Dickins, R. A. *et al.* Probing tumor phenotypes using stable and regulated synthetic microRNA precursors. *Nat. Genet.* **37,** 1289–1295 (2005).
43. Godar, S. *et al.* Growth-inhibitory and tumor- suppressive functions of p53 depend on its repression of *CD44* expression. *Cell* **134,** 62–73 (2008).
44. Dimri, G. P. *et al.* A biomarker that identifies senescent human cells in culture and in aging skin *in vivo*. *Proc. Natl Acad. Sci. USA* **92,** 9363–9367 (1995).
45. Reimann, M. *et al.* The Myc-evoked DNA damage response accounts for treatment resistance in primary lymphomas *in vivo*. *Blood* **110,** 2996–3004 (2007).
46. Greve, B., Kelsch, R., Spaniol, K., Eich, H. T. & Götte, M. Flow cytometry in cancer stem cell analysis and separation. *Cytometry A* **81A,** 284–293 (2012).
47. Gupta, P. B. *et al.* Identification of selective inhibitors of cancer stem cells by high-throughput screening. *Cell* **138,** 645–659 (2009).
48. Lu, D. *et al.* Salinomycin inhibits Wnt signaling and selectively induces apoptosis in chronic lymphocytic leukemia cells. *Proc. Natl Acad. Sci. USA* **108,** 13253–13257 (2011).
49. Kim, J. *et al.* A Myc network accounts for similarities between embryonic stem and cancer cell transcription programs. *Cell* **143,** 313–324 (2010).
50. Subramanian, A. *et al.* Gene set enrichment analysis: a knowledge-based approach for interpreting genome-wide expression profiles. *Proc. Natl Acad. Sci. USA* **102,** 15545–15550 (2005).
51. Rappsilber, J., Mann, M. & Ishihama, Y. Protocol for micro-purification, enrichment, pre-fractionation and storage of peptides for proteomics using StageTips. *Nat. Protocols* **2,** 1896–1906 (2007).
52. Boersema, P. J., Raijmakers, R., Lemeer, S., Mohammed, S. & Heck, A. J. Multiplex peptide stable isotope dimethyl labeling for quantitative proteomics. *Nat. Protocols* **4,** 484–494 (2009).
53. Cox, J. & Mann, M. MaxQuant enables high peptide identification rates, individualized p.p.b.-range mass accuracies and proteome-wide protein quantification. *Nat. Biotechnol.* **26,** 1367–1372 (2008).
54. Lee, T. I., Johnstone, S. E. & Young, R. A. Chromatin immunoprecipitation and microarray-based analysis of protein location. *Nat. Protocols* **1,** 729–748 (2006).
55. Hu, Y. & Smyth, G. K. ELDA: extreme limiting dilution analysis for comparing depleted and enriched populations in stem cell and other assays. *J. Immunol. Methods* **347,** 70–78 (2009).
56. Ivanova, N. B. *et al.* A stem cell molecular signature. *Science* **298,** 601–604 (2002).
57. Coppé, J. P., Desprez, P. Y., Krtolica, A. & Campisi, J. The senescence-associated secretory phenotype: the dark side of tumor suppression. *Annu. Rev. Pathol.* **5,** 99–118 (2010).
58. Whitfield, M. L. *et al.* Identification of genes periodically expressed in the human cell cycle and their expression in tumors. *Mol. Biol. Cell* **13,** 1977–2000 (2002).
59. Hu, Z. *et al.* The molecular portraits of breast tumors are conserved across microarray platforms. *BMC Genomics* **7,** 96 (2006).
60. Chambers, S. M. *et al.* Hematopoietic fingerprints: an expression database of stem cells and their progeny. *Cell Stem Cell* **1,** 578–591 (2007).

a

43 core ESC genes
181 ATSC genes

b

Gene set	Reference	ctrl;*Bcl2* NES	P	*Suv39h1⁻;Bcl2* NES	P
Cell cycle process	GO:0022402	-2.235	< 0.001	-1.827	< 0.001
Proliferation cluster	Ref. 58	-2.931	< 0.001	-1.858	< 0.001
Cycling genes	Ref. 59	-2.680	< 0.001	-1.692	< 0.001
ATSC	Ref. 17	2.511	< 0.001	0.915	0.790
core ESC	Ref. 49	1.012	0.435	1.105	0.284
HSC signature	Ref. 56	1.618	0.001	0.988	0.503
LT-HSC signature	Ref. 60	1.513	0.001	0.788	0.922

c

	Haematological malignancies				Colorectal cancers				Melanomas				B-CLL
	RCK8	Eheb	K562	Mec1	SW480	LS174T	DLD-1	Caco-2	WM266.4	SKMel28	MeWo	Omm2.3	Patient1
ut	9.7% ± 2.1	6.7% ± 1.5	14.7% ± 1.5	4.7% ± 1.2	4.3% ± 0.6	8.7% ± 0.6	4.7% ± 1.5	10.0% ± 1.0	4.0% ± 1.0	2.7% ± 0.6	8.3% ± 1.5	9.0% ± 2.0	18.4% ± 3.4
ADR	69.3% ± 2.1	60.7% ± 1.5	84.3% ± 4.2	7.7% ± 1.5	95.7% ± 2.1	77.0% ± 3.5	11.3% ± 1.5	15.7% ± 2.5	97.3% ± 2.1	91.7% ± 3.1	89.7% ± 2.1	10.7% ± 0.6	57.3% ± 8.7

d

e

f

g

Replicative stressor		Aging		Aging		Stasis, p16-dependent		Agonescence, telomere shortening	
Cell type		Mesenchymal stem cells		BJ - skin fibroblasts		Mammary epithelial cells		Mammary epithelial cells	
Gene set	Reference	NES	P	NES	P	NES	P	NES	P
Cell Cycle	GO:0022402	-4.154	<0.001	-1.282	0.032	-2.308	<0.001	-1.778	<0.001
ATSC	Ref.17	1.889	0.014	1.215	0.024	1.294	<0.001	1.847	<0.001

Extended Data Figure 1 | Senescent cells of mouse and human origin present with enhanced stem-cell markers and functionalities.

a, 5,401 probe sets (corresponding to 3,867 genes) differentially expressed in TIS were determined from the transcriptome data comparing untreated and ADR-senescent primary control;*Bcl2* lymphomas by two-way ANOVA adjusted for multiple testing (cut-off q < 0.05, n = 12 biologically independent samples). 181 out of 737 genes belonging to an ATSC[17] or 43 out of 337 genes of core embryonic stem-cell (ESC) signature[49] were detected and marked orange and blue, respectively, in the fold-change-ranked gene list. Whereas the expression of core embryonic stem-cell genes was not correlated with senescence, ATSC transcripts exhibit a strong association with TIS. **b**, Senescence-selective gene set enrichment pattern of proliferation- and stem-cell-related gene modules (including haematopoietic stem cell (HSC) and long-term HSC (LT-HSC) signatures)[56,58–60] in control;*Bcl2* and *Suv39h⁻;Bcl2* lymphoma cells as in Fig. 1a. GSEA based on the Kolmogorov–Smirnov test, with negative NES indicating enrichment in untreated lymphomas, and positive NES reflecting enrichment in TIS. n = 12 biologically independent control;*Bcl2* samples and n = 5 *Suv39h⁻;Bcl2* samples. NES of P < 0.05 are considered statistically significant and are shown in red. **c**, Senescence induction by ADR treatment in various human cell lines consisting of haematological malignancies, colorectal cancers, melanomas, or in primary samples from patients with B-CLL as determined by SA-β-gal staining (mean percentage of positive cells ± s.d., n = 3 independent experiments for cell lines; n = 4 individual B-CLL samples). TIS-competent cells are defined by a greater

than fourfold induction of SA-β-gal-positive cells (with the exception of B-CLL samples, in which SA-β-gal-positive cells were at least threefold induced), and depicted as a blue box symbol in Fig. 1c. **d**, ABC transporter activity in cells as in Fig. 1a, measured by the efflux of a fluorescent substrate with and without the ABC transporter inhibitor verapamil. Representative plots of four independent lymphomas tested per genotype. **e**, Enhanced expression of the stem-cell marker CD34 in the RCK8 cell line or primary human B-cell leukaemia samples exposed to ADR treatment *in vitro*. Mean fluorescence intensity ± s.d. from three independent experiments (RCK8 cells) and five individual leukaemia cases determined by flow cytometry. Two-tailed, unpaired t-test with Welch's correction, *P < 0.05. **f**, TIS-mediated increase and verapamil-dependent blockage of ABC transporter activity in ADR-senescent RCK8 cells and primary human B-cell leukaemia samples as in **e**. One representative out of three independent experiments shown. **g**, SAS occurring in non-malignant senescence scenarios: GSEA of proliferation- or stem-cell-related gene sets (as in **b**) in publicly available transcriptome data representing different models of replicative senescence: primary human mammary epithelial cells in stasis or agonescence (GSE16058, 12 prestasis, 9 stasis and 4 agonescence individual biological samples), high-passage BJ human skin fibroblasts (GSE13330, n = 6 pairs of proliferating/senescent cells from individual donors) or high-passage primary human mesenchymal stem cells (GSE9593, n = 3 pairs of proliferating/senescent cells from individual donors).
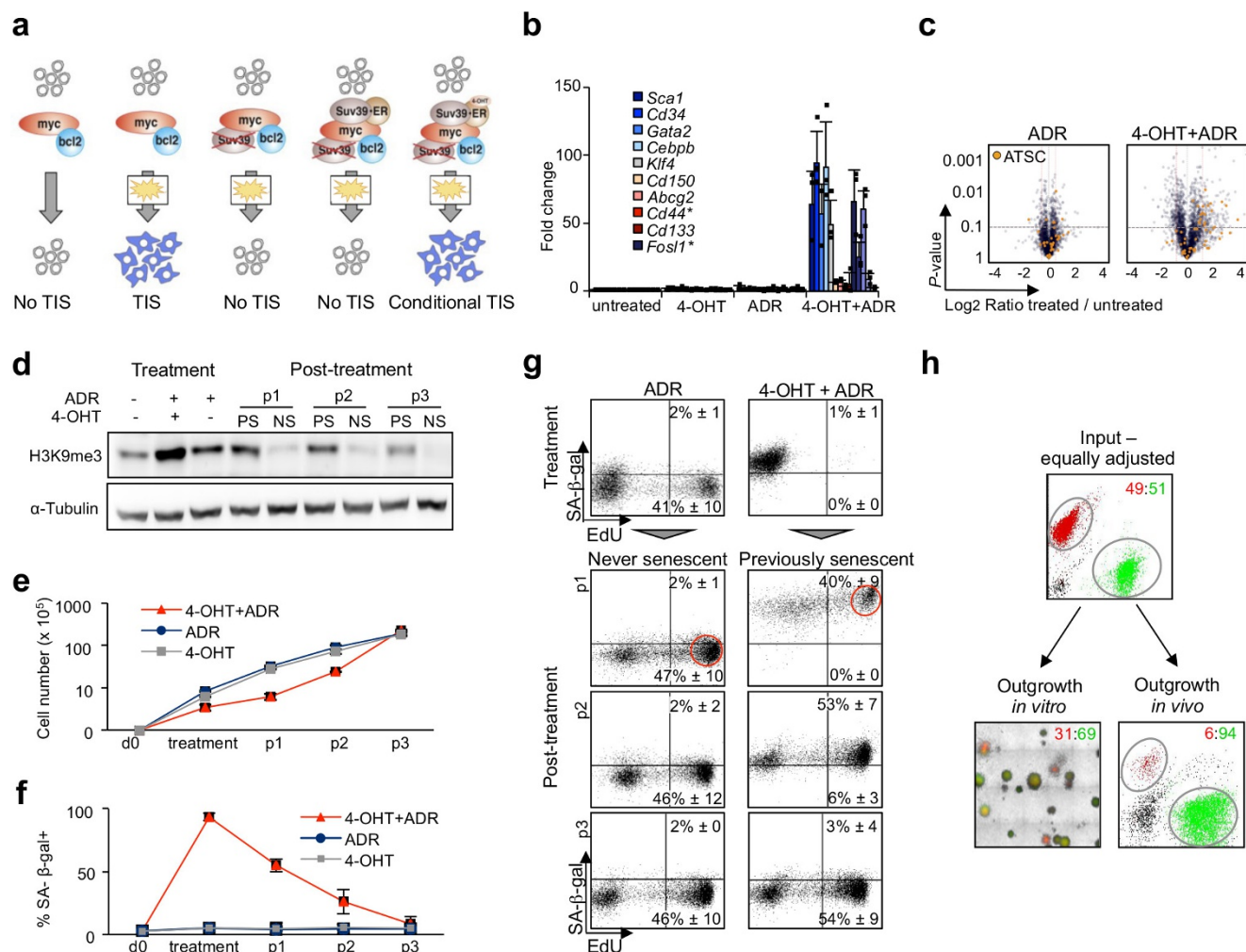
Extended Data Figure 2 | Genetic, biochemical and functional properties of regulatable senescence models. a, Graphic illustration of the model system engineered to stably express a regulatable senescence-essential gene moiety, such as $Suv39h1^-$ proficient and -deficient Eμ-*Myc* transgenic and *Bcl2*-infected lymphoma variants of which only $Suv39h1^-;Bcl2;Suv39h1$-ER^{T2} cells regain conditional TIS capability if exposed to 4-OHT. **b**, Relative transcript levels of the indicated stem-cell-related and Wnt target (asterisk) genes by qPCR in $Suv39h1^-;Bcl2;Suv39h1$-ER^{T2} lymphoma cells exposed to the indicated treatments for five days. Results represent mean fold induction relative to the untreated condition ± s.d. ($n = 3$ biologically independent samples). **c**, Global proteome analysis of total $Suv39h1^-;Bcl2;Suv39h1$-ER^{T2} cell lysates after five days of ADR ± 4-OHT treatment, showing mean protein expression changes relative to untreated condition (x axis) and their statistical significance (y axis), $n = 3$ biologically independent samples analysed by Wilcoxon test. All identifications with a $-\log_{10}$ transformed P value greater than 1 were considered significant. Dots representing ATSC factors are highlighted in orange. **d**, Immunoblot of H3K9me3 expression in $Suv39h1^-;Bcl2;Suv39h1$-ER^{T2} lymphoma cells treated as in **b** ('treatment'), and monitored at the indicated passages in 4-OHT/ADR-free medium ('post-treatment'; p1–3, each passage reflects 7 days in culture). Never senescent, ADR-only- and previously senescent ADR+4-OHT-pretreated lymphoma cells are analysed, α-tubulin is

used as a loading control. One out of two independent experiments shown. For gel source data, see Supplementary Fig. 1. **e**, **f**, Growth curve analysis (**e**) and SA-β-gal reactivity time course (**f**) of cells treated as in **d**. Results represent mean cell numbers or percentages of positive cells, respectively ± s.d., from three biologically independent samples. **g**, Kinetics of the proliferation marker EdU and the fluorescent SA-β-gal marker in $Suv39h1^-;Bcl2;Suv39h1$-ER^{T2} lymphoma cells after five days of ADR ± 4-OHT treatment ('treatment'), and subsequent passages in 4-OHT/ADR-free medium ('post-treatment', p1–3, each passage reflecting seven days in culture), demonstrating outgrowth of senescent (SA-β-gal$^+$) cells after terminating the 4-OHT/ADR treatment. Mean percentages of EdU$^+$/SA-β-gal$^+$ and EdU$^+$/SA-β-gal$^-$ cells ± s.d., $n = 4$ biologically independent samples. Representative photomicrographs from cell populations marked by red circles are shown in Fig. 2a. **h**, Competition assays of matched passage 2 previously senescent (GFP-labelled) and never senescent (DsRed-labelled) lymphomas plated at an equal ratio (top) and evaluated by fluorescence microscopy-scored colony formation *in vitro* (bottom left), and by flow cytometric analysis of lymphoma cells isolated from manifest tumours after transplantation (bottom right). Numbers reflect the ratio of red- to green-fluorescent colonies or cells, respectively. One representative out of four independent experiments shown, including colour reversal.
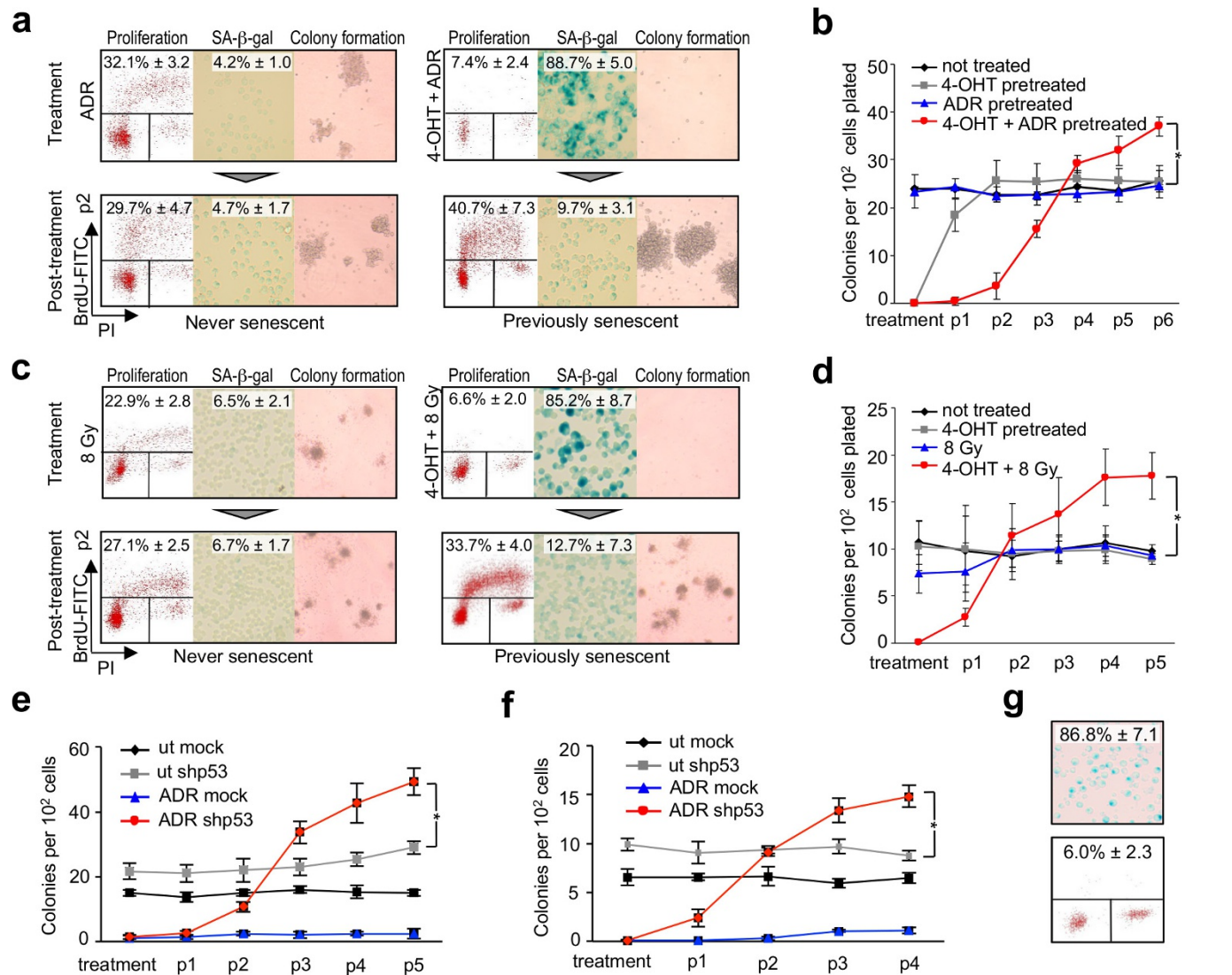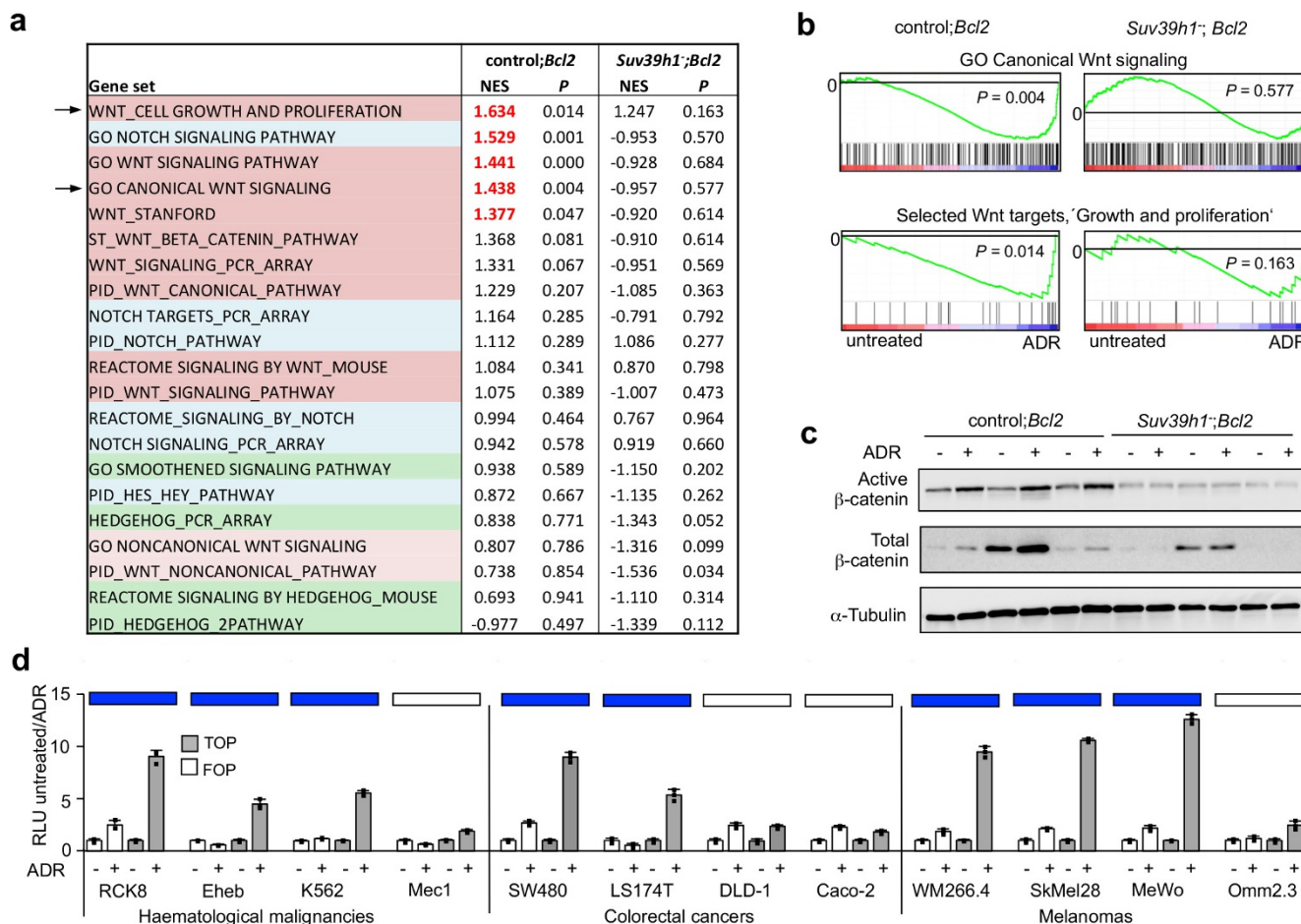
Extended Data Figure 3 | Senescence-released (previously senescent) cancer cells display higher tumour-initiating capacity than their never-senescent counterparts. a–d, Growth properties of conditionally senescent lymphoma cells analysed as in Fig. 2a, b, but using p53-ER^{Tam};*Bcl2* lymphoma cells with ADR ± 4-OHT treatment (**a, b**), or *Suv39h1^{-};Bcl2;Suv39h1*-ER^{T2} lymphoma cells exposed to a single dose of γ-irradiation (8 Gy) instead of ADR, followed by five days of 4-OHT treatment and subsequent passaging in 4-OHT-free medium (**c, d**). Results presented as mean positive cells or mean colony numbers ± s.d.; $n = 4$ (**a, c, d**) or $n = 3$ (**b**) biologically independent samples. Representative photomicrographs from one out of three independent experiments (**a, c**). Two-tailed, unpaired *t*-test with Welch's correction, comparing ADR- and 4-OHT+ADR pretreated lymphomas at p6, or 8 Gy- and 4-OHT+8 Gy at p5. *$P < 0.05$ (**b, d**). It is noteworthy that the superior growth and clonogenicity of post-senescent cells can be explained neither by rare cells that may simply have bypassed senescence, because the matching never senescent (that is, senescence bypasser) group presented with inferior clonogenicity, nor by an enhanced death rate of non-stem cells in the Suv39h1-proficient aliquot, because no significant differences in viability were observed between never senescent and previously senescent groups throughout these experiments. Viability determined by flow cytometry as thepercentage of annexin V/PI double-negative cells was typically greater than 80% and comparable between never senescent and previously senescent cells (not shown; the same applies for Figs 2a and 4a). Growth-promoting mutations are also unlikely, as senescent cells stopped replicating their DNA. **e, f,** Colony formation assay of untreated versus five-day-ADR-senescent human RCK8 lymphoma cells (**e**) or LT174T colon carcinoma cells (**f**) that were exposed to a shp53-lentivirus or mock infection on day five of ADR treatment, with *p53* knockdown enabling outgrowth out of fully established senescence. As observed for mouse lymphoma cells, post-senescent RCK8 and LT174T cells, after just three passages, outperformed the clonogenic potential of tumor cells that were equally exposed to shRNA against *p53* but never experienced senescence. Results represent mean colony numbers at indicated passages (each reflecting seven days in ADR-free methylcellulose medium) ± s.d., $n = 3$ independent experiments. Two-tailed, unpaired *t*-test with Welch's correction, comparing untreated shp53 versus ADR + shp53 at p5 (**e**) or p4 (**f**). *$P < 0.05$. **g,** TIS re-inducibility in *Suv39h1^{-};Bcl2;Suv39h1*-ER^{T2} previously senescent cells (at passage 2, compare with Fig. 2a) re-exposed to 4-OHT and ADR for five days, as detected by SA-β-gal staining (up) and BrdU/PI incorporation (down). Results represent mean percentages of positive cells ± s.d. ($n = 4$ independent lymphomas).
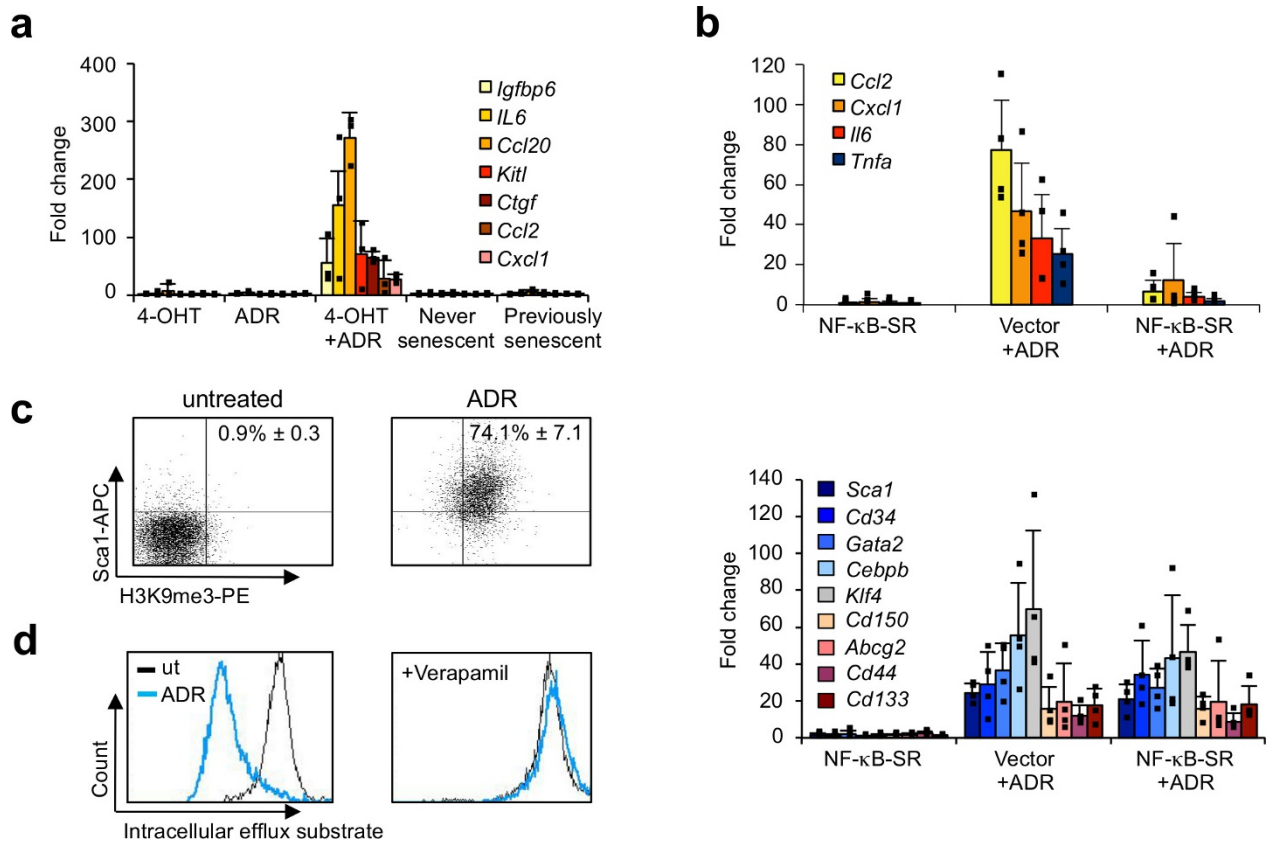
Extended Data Figure 4 | The senescence-associated secretory phenotype (SASP) is dispensable for senescence-associated stemness (SAS) induction. a, Expression of a panel of SASP transcripts[40,57] by qPCR in Suv39h1-regulatable lymphoma cells after five days of ADR ± 4-OHT exposure, and after two passages in 4-OHT/ADR-free medium (that is, in never senescent and previously senescent cells), showing SASP upregulation in TIS and its downregulation back to baseline levels in senescence-released previously senescent cells. Results represent mean fold induction relative to untreated lymphomas ± s.d. ($n = 3$ biologically independent samples). **b,** Blunting SASP production (top) by NF-κB super-repressor IκBαΔN (NF-κB-SR)-mediated genetic inhibition of NF-κB as the major SASP driver in TIS cells (without compromising their ability to enter TIS)[9,40] did not prevent acquisition of stemness markers

(bottom) by qPCR. Results represent mean fold induction relative to mock-transduced untreated cells ± s.d. ($n = 4$ biologically independent samples). **c,** Co-expression of the stem-cell marker Sca1 and the TIS marker H3K9me3 by flow cytometry in NF-κB-SR-expressing control;*Bcl2* cells exposed to ADR for five days, indicating uncompromised SAS induction. Percentages indicate mean Sca1/H3K9me3 double-positive cells ± s.d. ($n = 4$ biologically independent samples). **d,** ABC transporter activity by flow cytometry in control;*Bcl2*;NF-κB-SR cells as in **c**, again demonstrating strong induction of stem-cell-reminiscent ABC transporter activity in TIS cells (compare with Extended Data Fig. 1d) irrespective of their blunted SASP response. Representative plots out of four independent lymphomas shown.

a

Gene set	control;*Bcl2*		*Suv39h1⁻*;*Bcl2*	
	NES	P	NES	P
→ WNT_CELL GROWTH AND PROLIFERATION	**1.634**	0.014	1.247	0.163
GO NOTCH SIGNALING PATHWAY	**1.529**	0.001	-0.953	0.570
GO WNT SIGNALING PATHWAY	**1.441**	0.000	-0.928	0.684
→ GO CANONICAL WNT SIGNALING	**1.438**	0.004	-0.957	0.577
WNT_STANFORD	**1.377**	0.047	-0.920	0.614
ST_WNT_BETA_CATENIN_PATHWAY	1.368	0.081	-0.910	0.614
WNT_SIGNALING_PCR_ARRAY	1.331	0.067	-0.951	0.569
PID_WNT_CANONICAL_PATHWAY	1.229	0.207	-1.085	0.363
NOTCH TARGETS_PCR_ARRAY	1.164	0.285	-0.791	0.792
PID_NOTCH_PATHWAY	1.112	0.289	1.086	0.277
REACTOME SIGNALING BY WNT_MOUSE	1.084	0.341	0.870	0.798
PID_WNT_SIGNALING_PATHWAY	1.075	0.389	-1.007	0.473
REACTOME_SIGNALING_BY_NOTCH	0.994	0.464	0.767	0.964
NOTCH SIGNALING_PCR_ARRAY	0.942	0.578	0.919	0.660
GO SMOOTHENED SIGNALING PATHWAY	0.938	0.589	-1.150	0.202
PID_HES_HEY_PATHWAY	0.872	0.667	-1.135	0.262
HEDGEHOG_PCR_ARRAY	0.838	0.771	-1.343	0.052
GO NONCANONICAL WNT SIGNALING	0.807	0.786	-1.316	0.099
PID_WNT_NONCANONICAL_PATHWAY	0.738	0.854	-1.536	0.034
REACTOME SIGNALING BY HEDGEHOG_MOUSE	0.693	0.941	-1.110	0.314
PID_HEDGEHOG_2PATHWAY	-0.977	0.497	-1.339	0.112

b

c

d

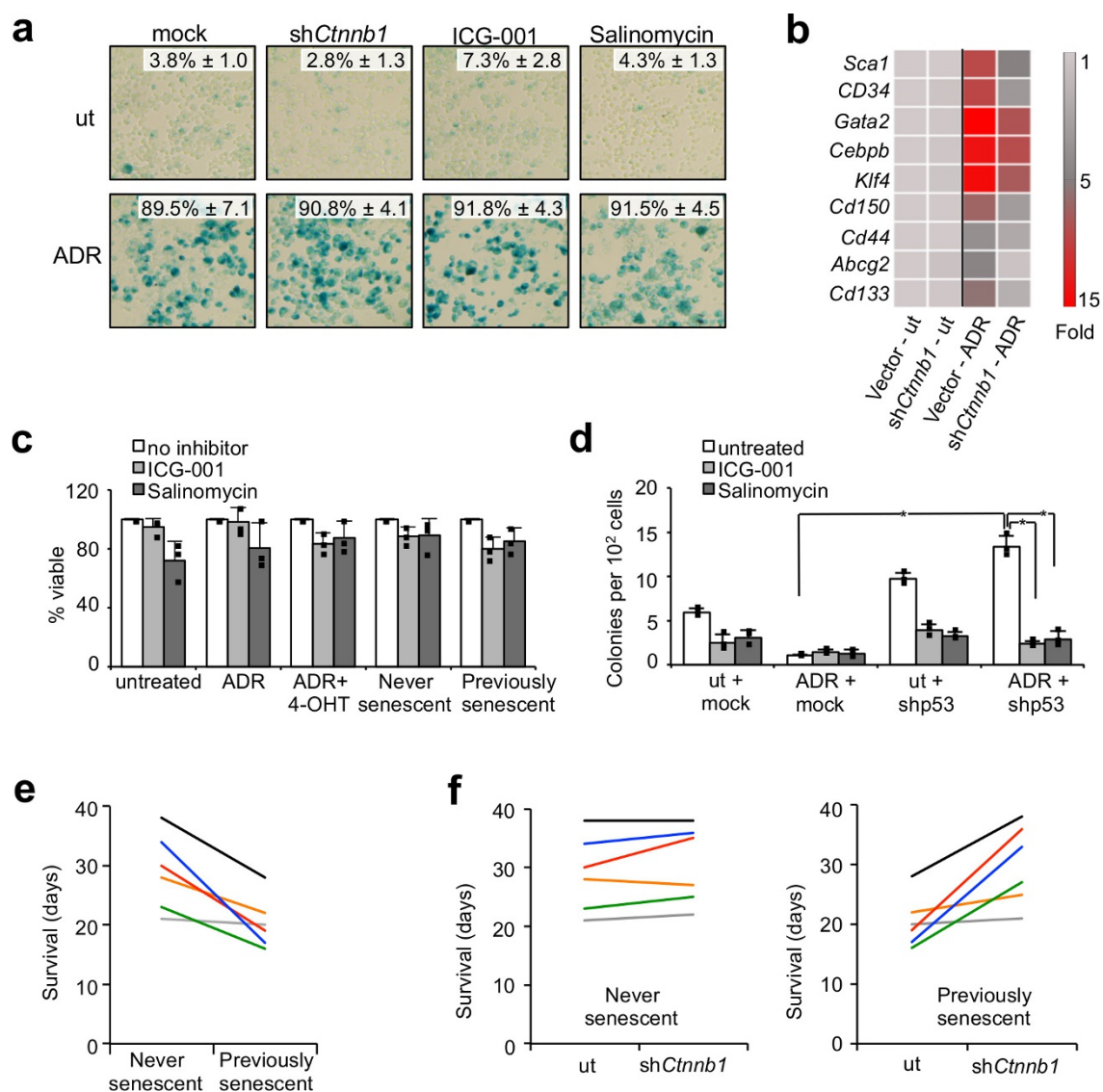**Extended Data Figure 5 | Wnt signalling is upregulated in senescence.** **a**, GSEA of gene sets probing stem-cell-relevant signalling pathways in ADR-senescent control;*Bcl2* or TIS-incompetent *Suv39h1⁻*;*Bcl2* cells (as in Fig. 1a). Positive NES indicate enrichment in TIS lymphomas. NES of $P < 0.05$ are considered statistically significant and are presented in red. $n = 12$ pairs of independent lymphomas. **b**, GSEA enrichment plots of selected gene sets presented in **a**; GO term 'Canonical Wnt receptor signaling' (top) or subset of proliferation-relevant Wnt target genes (bottom), showing significant enrichment in ADR-senescent control;*Bcl2* but not in TIS-incompetent *Suv39h1⁻*;*Bcl2* cells. **c**, Immunoblot analysis of Ser37- and Thr41-dephosphorylated (that is, stabilized and nucleus

translocation-capable 'Active β-catenin') and total β-catenin in three independent pairs of control;*Bcl2* and *Suv39h1⁻*;*Bcl2* lymphoma cells, exposed to ADR for 5 days (+) or left untreated (−). α-Tubulin is used as a loading control. One out of two independent experiments shown. For gel source data, see Supplementary Fig. 1. **d**, Wnt activity measured by the TOPflash TCF reporter system (with FOPflash as negative control) in human cell lines in correlation with their senescence inducibility by ADR, as indicated by blue box symbols for senescence-competent cell lines (referring to Extended Data Fig. 1c). Results reflect mean relative light units fold change (between untreated and ADR-treated samples) of three independent experiments ± s.d.
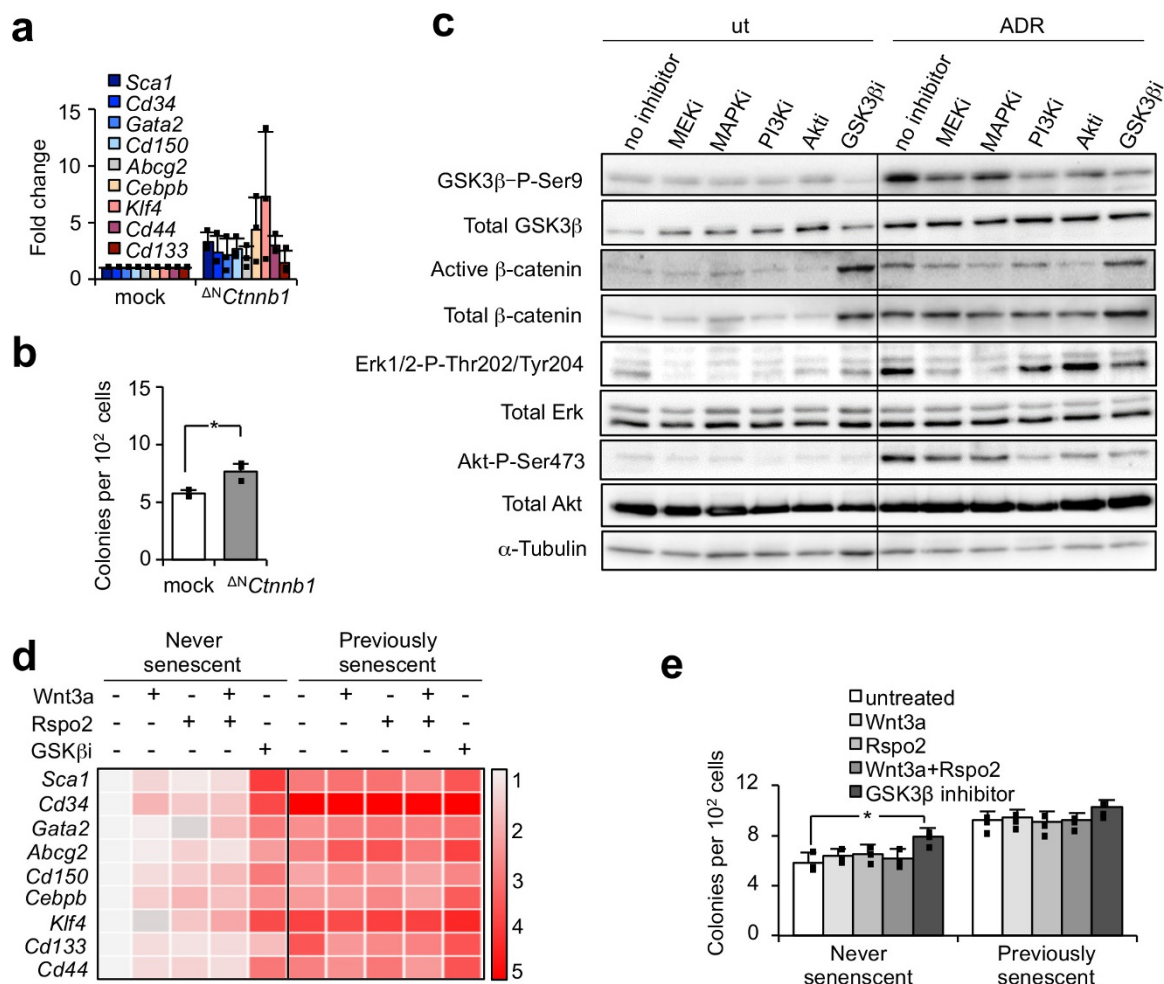
Extended Data Figure 6 | Cell-intrinsic activation of Wnt signalling cascade in TIS. a, b, Expression of indicated stem-cell-related transcripts by qPCR (**a**) and colony formation (**b**) in control;*Bcl2* lymphomas infected with a constitutively active Ctnnb1 mutant (△NCtnnb1) or a mock retrovirus. Data represent mean expression fold change normalized to mock-infected cells and mean colony numbers, respectively ± s.d. (*n* = 3 biologically independent samples). Two-tailed, unpaired *t*-test with Welch's correction. *$P < 0.05$. **c**, Immunoblot analysis of Ser9-phosphorylated (that is, inactivated) or total GSK3β, active or total β-catenin (as in Extended Data Fig. 5c), Thr202- and Tyr204-phosphorylated or total Erk1/2, and Ser473-phosphorylated or total Akt in control;*Bcl2* lymphoma cells treated with ADR for five days, together with pharmacological inhibitors targeting MAPK and PI3K kinase pathways.

α-Tubulin was used as a loading control. One out of two independent experiments shown. For gel source data, see Supplementary Fig. 1. **d**, Expression of the indicated stem-cell-related transcripts by qPCR in never senescent and previously senescent *Suv39h1⁻;Bcl2;Suv39h1*-ER^T2 cells (passage 2) exposed to Wnt signalling agonists (Wnt3a, Rspo2, or GSK3β inhibitor) for two days. Colour scale represents mean fold change normalized to never senescent cells not exposed to Wnt agonists ± s.d. (*n* = 3 individual lymphomas). **e**, Colony formation of never senescent and previously senescent cells (as in **d**), after seven days in methylcellulose medium supplemented with the indicated Wnt agonists (mean colony numbers ± s.d., *n* = 3 individual lymphomas). Two-tailed, unpaired *t*-test with Welch's correction. *$P < 0.05$.

Extended Data Figure 7 | Wnt signalling is dispensable for senescence induction, but required for senescence-associated stemness.
a, Senescence induction by ADR in control;*Bcl2* lymphoma cells with and without parallel application of the indicated pharmacological or genetic Wnt inhibitors (ICG-001, salinomycin or *Ctnnb1* knockdown by shRNA (shCtnnb1)). Results reflect mean percentages of SA-β-gal-positive cells ± s.d. (*n* = 4 independent lymphomas). **b**, Expression of stemness-related transcripts by qPCR in ADR-treated control;*Bcl2* lymphoma cells exposed to *Ctnnb1* knockdown by shRNA retroviral infection (shCtnnb1). The colour scale represents mean fold induction normalized to ADR-untreated (ut) and vector-infected controls ± s.d. (*n* = 3 biologically independent samples). **c**, Relative viability of *Suv39h1⁻;Bcl2;Suv39h1*-ER^T2 cells exposed to the indicated Wnt inhibitors either simultaneously with ADR ± 4-OHT treatment (for the last 48 h of treatment), or at passage 2 after terminating ADR ± 4-OHT (never senescent and previously senescent; treated over 48 h with inhibitors).

Results show relative viability normalized to sample with no Wnt inhibitor treatment ± s.d. (*n* = 3 biologically independent samples). **d**, Colony formation of human LT174T colon carcinoma cells exposed to mock or shp53-lentivirus upon ADR-induced senescence, and further propagated in ADR-free medium (corresponding to passage 3 in Extended Data Fig. 3f). Results show mean colony counts after seven-day exposure to indicated Wnt inhibitors ± s.d. (*n* = 3 independent experiments per group). Two-tailed, unpaired *t*-test with Welch's correction, *$P < 0.05$. **e**, Individual survival times of the six matched never senescent and previously senescent lymphoma pairs (shown collectively in Fig. 3d). **f**, Individual survival times of mice bearing never senescent (left) and previously senescent lymphomas (right) after exposure to Wnt signalling inhibition by *Ctnnb1* knockdown (shCtnnb1) or left uninhibited. The line plots represent the same matched never senescent and previously senescent lymphomas as in **e**.
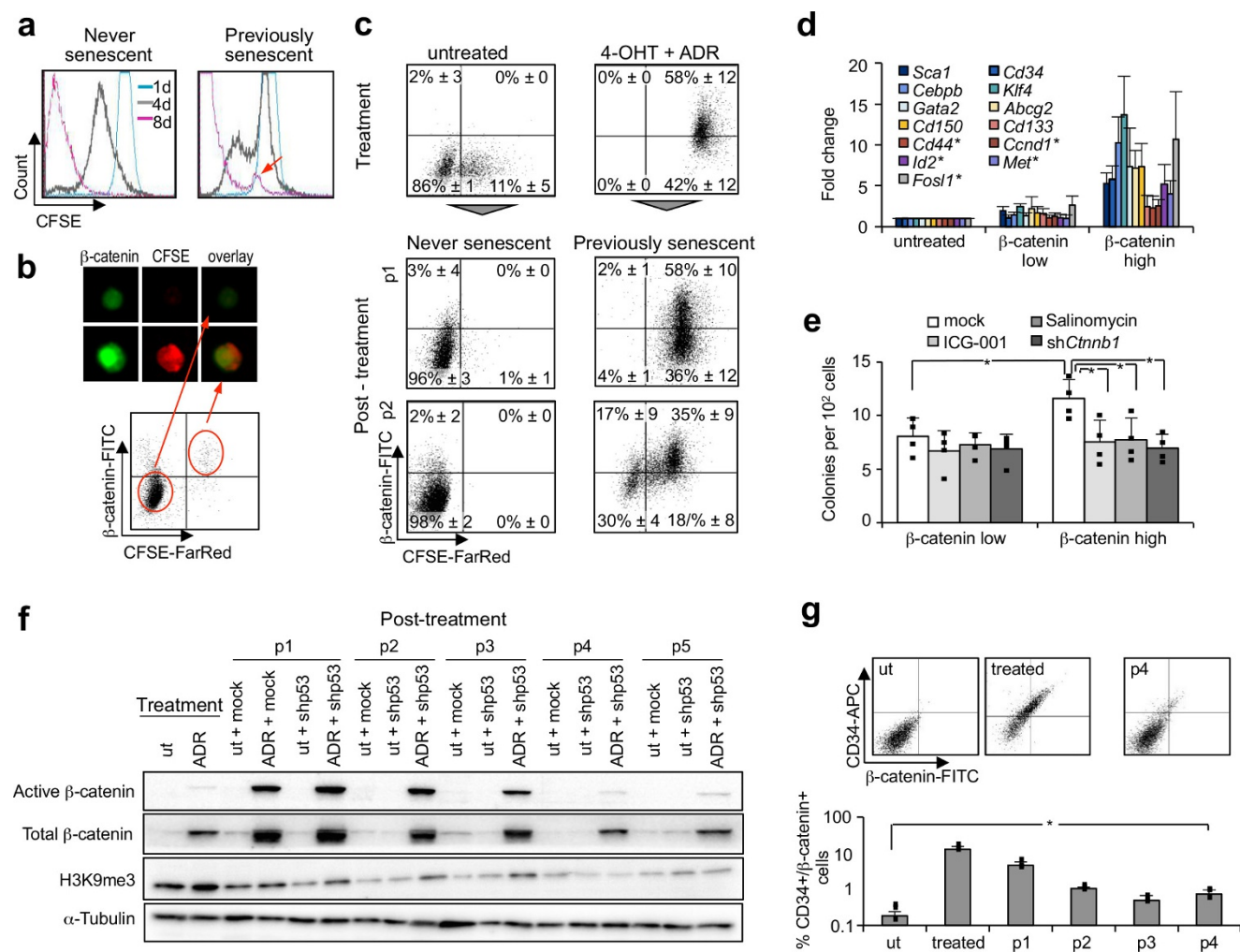
Extended Data Figure 8 | The previously senescent cell population maintains a stable fraction of Wnt-active stem cells over time.
a, Detection of a slowly dividing subpopulation in previously senescent but not in never senescent lymphoma cells (arrow) by the CFSE membrane dye 1, 4 or 8 days after stopping the ADR ± 4-OHT treatment. Experiment performed in triplicates. **b**, CFSE[high] previously senescent cells exhibited more profound nuclear β-catenin expression, indicating acquired stemness (passage 3 after 4-OHT/ADR removal; compare with **c**). One out of three independent experiments, each performed in triplicate. **c**, Co-staining with β-catenin and CFSE as in **b** in *Suv39h1[−];Bcl2;Suv39h1*-ER[T2] cells, untreated or exposed to ADR ± 4-OHT for five days ('treatment') and subsequently passaged in 4-OHT/ADR-free medium (p1–2; each passage reflects seven days in culture). The slowly cycling (CFSE[high]) population was positive for β-catenin and persisted over time, although their relative percentage drops owing to outgrowth of their (CFSE[low]) progeny. Numbers reflect mean percentages from three independent lymphomas ± s.d. **d**, **e**, Higher expression of ATSC- or Wnt-related (asterisks) transcripts by qPCR (**d**) and higher clonogenic capacity, which can be neutralized by indicated pharmacological or genetic Wnt inhibitors (**e**) in flow-sorted, β-catenin high versus β-catenin low previously senescent cells (passage 3 after 4-OHT/ADR removal). Mean expression levels normalized to

untreated cells and mean colony numbers respectively ± s.d., $n = 4$ biologically independent samples. Two-tailed, unpaired *t*-test with Welch's correction, *$P < 0.05$. **f**, Immunoblot analysis of β-catenin and H3K9me3 levels in human RCK8 lymphoma cells exposed to ADR for 5 days to induce senescence ('treatment'), then stably transduced with an shp53- or mock lentivirus, and further propagated in ADR-free medium ('post-treatment', p1–5, each reflecting seven days in culture). The senescence-associated high levels of active and total β-catenin achieve a low but stable level at later passages. It is noteworthy that stably senescent ADR-pretreated, mock-infected cells were only blotted in p1. One representative out of three independent experiments shown, with α-tubulin as a loading control. For gel source data, see Supplementary Fig. 1. **g**, Co-expression of β-catenin and the stem-cell marker CD34 detected by flow cytometry in ADR-pretreated, shp53-infected RCK8 cells as in **f**, demonstrating a small but stable steady-state fraction of double-positive cells at later passages, explaining the lastingly enhanced colony-forming potential of previously senescent versus never senescent cells. Representative flow cytometry plots from three independent experiments (top) and mean percentages of double-positive cells ± s.d. (bottom) at the indicated passages ($n = 3$ independent experiments). Two-tailed, unpaired *t*-test with Welch's correction. *$P < 0.05$.
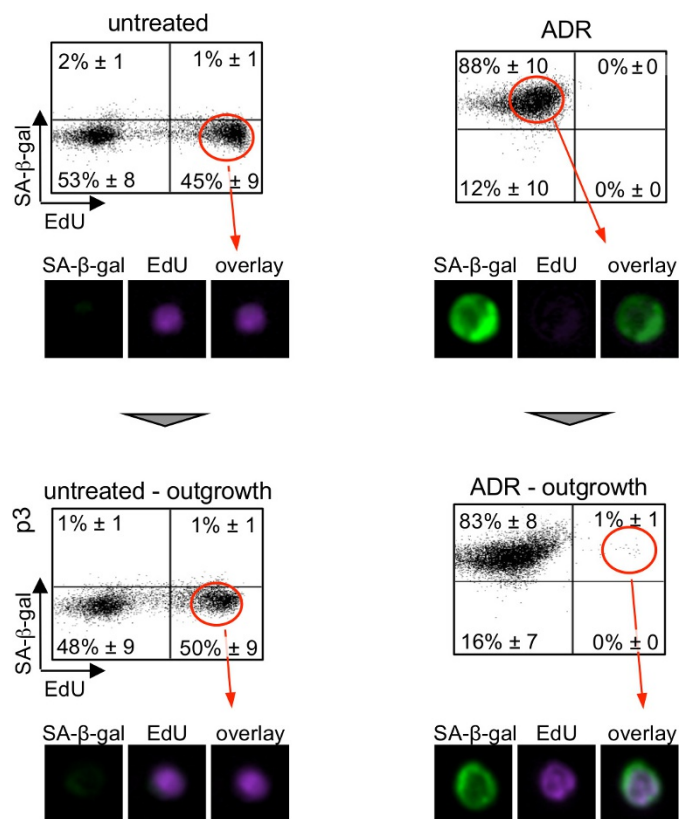
Extended Data Figure 9 | Spontaneous escape out of senescence detected in cancer cells without genetic manipulations of senescence-relevant genes. Flow cytometric analysis of the proliferation marker EdU and a fluorescent SA-β-gal marker in control;*Bcl2* cells treated with ADR or left untreated (top), and further cultivated in ADR-free medium (bottom). Co-expression of EdU in a small population of still SA-β-gal-positive cells demonstrates the ability of some ADR-senescent cells to escape the senescence arrest. Numbers represent mean percentages ± s.d. from four independent lymphomas. Photomicrographs depict representative cells from populations marked with red circles ($n = 4$ independent experiments).
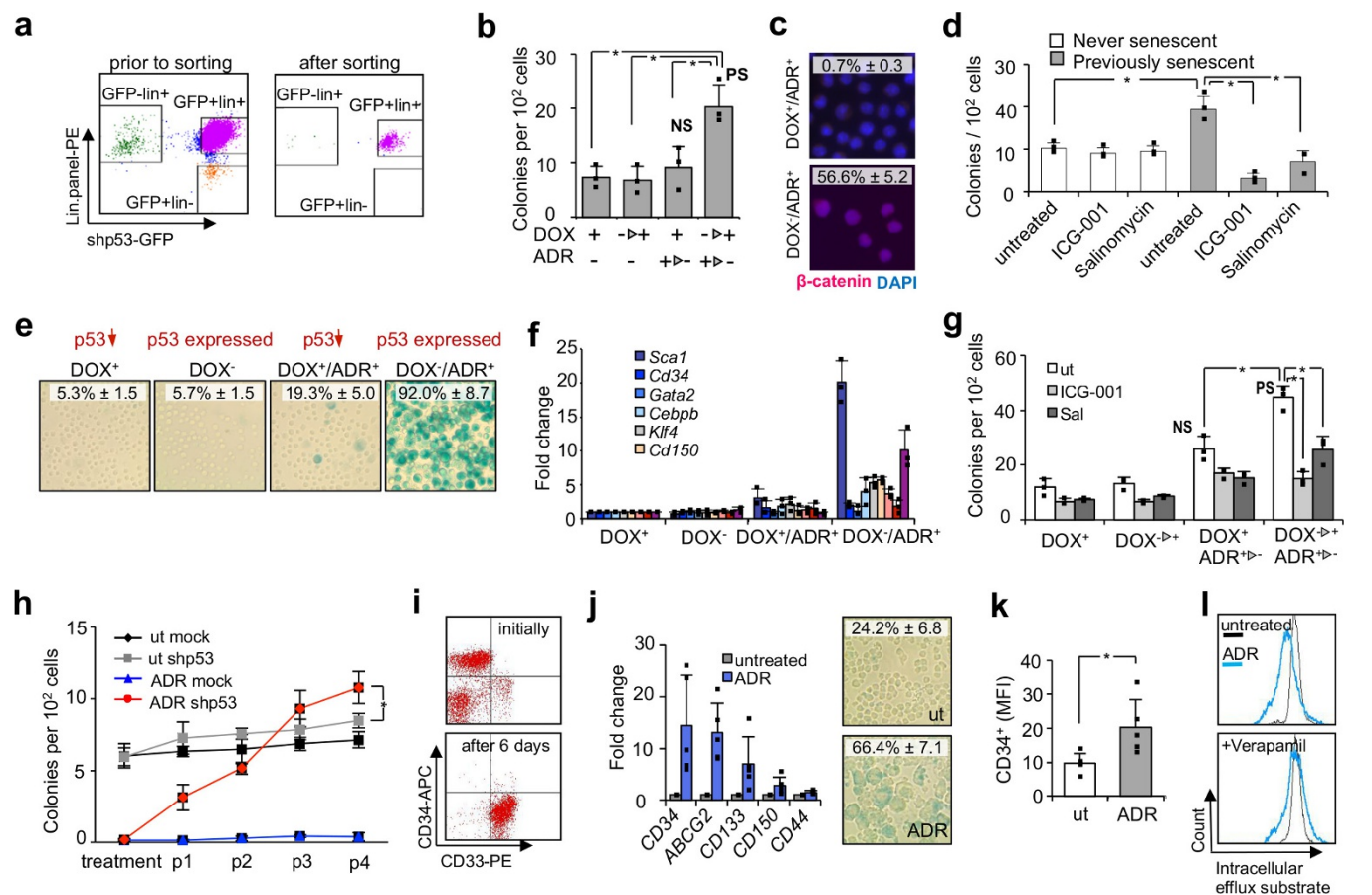
Extended Data Figure 10 | Senescence-associated *de novo* generation of leukaemia stem cells upon depletion of the stem-cell-containing fraction in mouse and human leukaemia samples. a, Flow cytometry plots of mouse *Kras*[G12D];DOX-on-shp53–GFP-induced T-cell acute lymphoblastic leukaemias (total splenocytes after short-term culture and retroviral *Bcl2* infection), stained with a panel of mouse lineage antibodies before and after flow-based sorting of the Lin[+]GFP[+] population. The Lin[−]GFP[+] population (including Kit[+]Sca1^{+} leukaemia stem cells) was used as a positive control. Shown are representative plots ($n = 3$). **b**, Colony formation of mouse Lin[+]GFP^{+} leukaemia cells as in **a**, pretreated with ADR ± doxycycline (DOX) for five days and subsequently seeded in ADR-free/DOX-supplemented medium, thus producing never senescent and previously senescent cells, respectively. Results represent mean colony counts at passage 2 (each passage reflecting 10 days in culture) ± s.d. ($n = 3$ biologically independent samples). Two-tailed, unpaired *t*-test with Welch's correction. *$P < 0.05$. **c**, Nuclear β-catenin expression by immunofluorescence (in red) in equally five-day-ADR-exposed senescent versus non-senescent settings (that is, DOX[−] versus DOX[+]). DAPI was used as a nuclear counterstain (in blue). Numbers represent mean percentages of β-catenin-positive cells ± s.d. ($n = 3$ biologically independent samples). **d**, Colony formation of never senescent and previously senescent leukaemia cells pretreated as in **b** (passage 3) with the addition of the indicated pharmacological Wnt inhibitors (mean colony numbers ± s.d., $n = 3$ biologically independent samples per group). *$P < 0.05$, two-tailed, unpaired *t*-test with Welch's correction. **e**, Senescence induction by SA-β-gal staining in mouse *Nras*[G12D];MLL-AF9;DOX-on-shp53;*Bcl2* bulk AML cells (Lin[−]Kit[+]Sca1^{+}-depleted) after five days of the ADR ± DOX treatment. Numbers reflect mean percentages of SA-β-gal-positive cells ± s.d (experiment performed in triplicate). Notably, viability determined as the percentage of annexin V/PI double-negative cells was typically greater than 80% and comparable between treatment groups. **f**, Stemness-related transcripts by qPCR in conditionally senescent mouse AML cells as in **e**. Graphs represent

mean fold induction ± s.d. ($n = 3$ independent experiments). **g**, Colony formation of mouse bulk leukaemia cells pretreated as in **e**, further propagated in ADR-free DOX-containing medium for 14 days, and plated in methylcellulose medium supplemented with the Wnt inhibitors ICG-001 or salinomycin. Colonies were counted after seven days. Previously senescent AML cells, emerging via DOX-mediated p53 knockdown, presented with the highest, Wnt-dependent clonogenicity, which could be attenuated by pharmacological Wnt inhibition. Results represent mean colonies ± s.d. ($n = 3$ independent experiments). Two-tailed, unpaired *t*-test with Welch's correction. *$P < 0.05$. **h**, Colony formation of the CD34^{+} cell-depleted human AML cell line Molm13 (with constitutive retroviral *Bcl2*-expression) exposed to senescence-inducing ADR treatment for five days ('treatment') and subsequently transduced with the lentiviral shp53 or mock construct (p53-knockdown enabling outgrowth from fully established senescence). Results reflect mean colony numbers ± s.d. ($n = 3$ independent experiments). Two-tailed, unpaired *t*-test with Welch's correction. *$P < 0.05$. **i**, Flow cytometric detection of the CD33 myeloid differentiation marker and CD34 stem-cell marker surface expression in samples from patients with AML obtained at diagnosis, before any cell cultivation and after six days of cultivation *in vitro*. Representative plots are shown ($n = 5$ individual patient samples). **j**, Expression of stemness-related transcripts in five-day-ADR-senescent versus untreated, *ex vivo* CD34^{+}-depleted primary human AML cells as in **i** (qPCR; average fold induction ± s.d., $n = 5$ individual patient samples, left). Photomicrographs (right) confirm ADR-inducible senescence by SA-β-gal staining (mean percentages of SA-β-gal positive cells ± s.d., representative photomicrographs from five independent samples). **k**, Regained CD34 surface expression upon ADR-induced senescence in CD34^{+}-depleted primary human AML cells as presented in **j**. Numbers reflect mean fluorescence intensity detected by flow cytometry ± s.d. ($n = 5$ individual patient samples). Two-tailed, paired *t*-test, *$P < 0.05$. **l**, ABC transporter activity in ADR-senescent versus untreated cells as in **k**. Representative plots are shown ($n = 5$ individual samples).

nature research

Corresponding author(s):   Clemens A. Schmitt

☐ Initial submission   ☐ Revised version   ☒ Final submission

Life Sciences Reporting Summary

Nature Research wishes to improve the reproducibility of the work that we publish. This form is intended for publication with all accepted life science papers and provides structure for consistency and transparency in reporting. Every life science submission will use this form; some list items might not apply to an individual manuscript, but all fields must be completed for clarity.

For further information on the points included in this form, see Reporting Life Sciences Research. For further information on Nature Research policies, including our data availability policy, see Authors & Referees and the Editorial Policy Checklist.

▶ Experimental design

1. Sample size

Describe how sample size was determined.

> Based on previous experience with the Eµ-myc transgenic mouse lymphoma model, sample sizes typically reflect three to five individual primary tumors as independent biological replicates. For assessing long-term outcome after in vivo-treatments, six or more tumor-bearing animals per arm were used.

2. Data exclusions

Describe any data exclusions.

> No data were excluded, all probes/animals that met proper experimental conditions were included in the analysis.

3. Replication

Describe whether the experimental findings were reliably reproduced.

> All experimental findings were reliably reproduced.

4. Randomization

Describe how samples/organisms/participants were allocated into experimental groups.

> No randomization was used to allocate experimental groups.

5. Blinding

Describe whether the investigators were blinded to group allocation during data collection and/or analysis.

> No blinding was used during allocation of experimental groups.

Note: all studies involving animals and/or human research participants must disclose whether blinding and randomization were used.

6. Statistical parameters

For all figures and tables that use statistical methods, confirm that the following items are present in relevant figure legends (or in the Methods section if additional space is needed).

n/a	Confirmed	
☐	☒	The exact sample size (n) for each experimental group/condition, given as a discrete number and unit of measurement (animals, litters, cultures, etc.)
☐	☒	A description of how samples were collected, noting whether measurements were taken from distinct samples or whether the same sample was measured repeatedly
☐	☒	A statement indicating how many times each experiment was replicated
☐	☒	The statistical test(s) used and whether they are one- or two-sided (note: only common tests should be described solely by name; more complex techniques should be described in the Methods section)
☐	☒	A description of any assumptions or corrections, such as an adjustment for multiple comparisons
☐	☒	The test results (e.g. P values) given as exact values whenever possible and with confidence intervals noted
☐	☒	A clear description of statistics including central tendency (e.g. median, mean) and variation (e.g. standard deviation, interquartile range)
☐	☒	Clearly defined error bars

See the web collection on statistics for biologists for further resources and guidance.

▶ Software

Policy information about availability of computer code

7. Software

Describe the software used to analyze the data in this study.

The data were analyzed by Microsoft Office Excel 2013 or Prism GraphPad 5. The limiting dilution tumor initiation data were analyzed by ELDA software (http://bioinf.wehi.edu.au/software/elda/). The gene enrichment analysis was performed using GSEA v2.0 software (http://www.broad.mit.edu/gsea). The global proteome processing was aided by using Chronos software package (Axel Semrau) and data analyzed using MaxQuant software version 1.2.2.5 (Ref. 53) and R-statistical software (https://www.r-project.org/).

For manuscripts utilizing custom algorithms or software that are central to the paper but not yet described in the published literature, software must be made available to editors and reviewers upon request. We strongly encourage code deposition in a community repository (e.g. GitHub). *Nature Methods* guidance for providing algorithms and software for publication provides further information on this topic.

▶ Materials and reagents

Policy information about availability of materials

8. Materials availability

Indicate whether there are restrictions on availability of unique materials or if these materials are only available for distribution by a for-profit company.

No restrictions on reagent availibility

9. Antibodies

Describe the antibodies used and how they were validated for use in the system under study (i.e. assay and species).

Antibodies against total ?-catenin (BD Biosciences, cat. no. 610153, 1:200, species reactivity: Hu (QC testing), M, R, D; application: WB (routinely tested), ICH, IP, IF (tested during development)), active ?-catenin (dephosphorylated at serine 37 [Ser37] and threonine 41 [Thr41]; Millipore, cat. no. 05-665, 1:1000, species reactivity: Hu, M, R; application: FC, ICC, IHC, IH(P), WB), H3K9me3 (Abcam, ab8898, 1:2,000, species reactivity: mammal, S. cerevisae, X. laevis, D. melanogaster; tested for applications: IHC, ICC, WB, FC, ChIP, ChIPseq), total Erk (Cell Signaling Technology [CST], cat. no. 9102, 1:1000, species reactivity: Hu, M, R, H, Monkey, Mink, Zebrafish, Bovine, Pig, S. cerevisiae; tested application: WB, IP, ICH), phospho-Erk1/2 (i.e. Erk1/2-P-Thr202/Tyr204; CST, cat. no. 4376, 1:1000, species reactivity: Hu, M, R, Hm, Monkey, Mink, Zebrafish, Pig, S. cerevisiae; tested application: WB, IP, ICH), total Akt (CST, cat. no. 9272, 1:1000, species reactivity: Hu, M, R, Hm, Monkey, Mink, Zebrafish, Bovine, Pig, S. cerevisiae; tested application: WB, IP, ICH, FC), phospho-Akt (i.e. Akt-P-Ser473; CST, cat. no. 4060, 1:2000, species reactivity: H, M, R, Monkey; tested application: WB, IP, ICH, IF, FC), total GSK3? (CST, cat. no. 12456, 1:1000, species reactivity: H, M, R, Monkey; tested application: WB, IP, ICH, IF, FC), phospho-GSK3? (i.e. GSK3?-P-Ser9; CST, cat. no. 5558, 1:1000, species reactivity: Hu, M, R, Hm; tested application: WB, IP, IF, FC) and α-Tubulin (Sigma, T5168, 1:1000, species reactivity: Hu, M, R, Monkey, Chicken, Kangaroo, Sea Urchin; tested application: WB, RIA, IF) were used in this study.

10. Eukaryotic cell lines

a. State the source of each eukaryotic cell line used.

Human cancer cell lines were obtained from DSMZ (Leibniz-Institut Deutsche Sammlung von Mikroorganismen und Zellkulturen GmbH), ATCC or Biomol: RCK8 (DSMZ-No. ACC-561), Eheb (DSMZ-No. ACC-67), K562 (DSMZ-No. ACC-10), Mec1 (DSMZ-No. ACC-497), Molm13 (DSMZ-No. ACC-554), SW480 (DSMZ-No. ACC-313), LS174T (DSMZ-No. ACC-759), DLD-1 (DSMZ-No. ACC-278), Caco-2 (DSMZ-No. ACC-169), SKMel28 (ATCC No. HTB-72), MeWo (ATCC No. HTB-65), WM266.4 (Biomol No. WM266-4-01). Omm2.3 cells were kindly provided by Martina J. Jager.

b. Describe the method of cell line authentication used.

The cell lines bought within last 4 years were not additionally authenticated (RCK8, Eheb, Mec-1, purchased at DSMZ in December 2013, authentication by nanoplex PCR of short tandem repeat markers provided by the distributor). All other cell lines were authenticated by DSMZ using SNP-based multiplex approach in October 2017. SNP profiles matched known profiles or were unique.

c. Report whether the cell lines were tested for mycoplasma contamination.

The cell lines regularly tested for mycoplasma contamination.

d. If any of the cell lines used are listed in the database of commonly misidentified cell lines maintained by ICLAC, provide a scientific rationale for their use.

None of the cell lines used are listed in the ICLAC list.

▶ Animals and human research participants

Policy information about studies involving animals; when reporting animal research, follow the ARRIVE guidelines

11. Description of research animals

Provide details on animals and/or animal-derived materials used in the study.

6–8-week-old C57BL/6 ("wild type") female mice were used as recipients for in vivo lymphoma or leukemia propagation.

Policy information about studies involving human research participants

12. Description of human research participants

Describe the covariate-relevant population characteristics of the human research participants.

The tumor biopsies from five B-cell leukemia patients (age 60-72 years, all male, initial diagnosis or relapse biopsies), five diffuse large B-cell lymphoma [DLBCL] patients (age 49-77 years, three females and two males, matched pairs of initial diagnosis and relapse biopsies) and acute myeloid leukemia [AML] patients (age 33-83 years, four females and one male, initial diagnosis) were used in this study.

nature research

Corresponding author(s):   Clemens A. Schmitt

☐ Initial submission   ☐ Revised version   ☒ Final submission

Flow Cytometry Reporting Summary

Form fields will expand as needed. Please do not leave fields blank.

▶ Data presentation

For all flow cytometry data, confirm that:

☒ 1. The axis labels state the marker and fluorochrome used (e.g. CD4-FITC).

☐ 2. The axis scales are clearly visible. Include numbers along axes only for bottom left plot of group (a 'group' is an analysis of identical markers).

☒ 3. All plots are contour plots with outliers or pseudocolor plots.

☒ 4. A numerical value for number of cells or percentage (with statistics) is provided.

▶ Methodological details

5. Describe the sample preparation.	Please see Methods, Generation of primary lymphomas and leukemias, page 19
6. Identify the instrument used for data collection.	The data were acquired using FACS Calibur™ (BD Biosciences) or ImageStream®X Mark II (AMNIS®, Merck Millipore). The sample sorting was performed using FACS Aria II (BD Biosciences).
7. Describe the software used to collect and analyze the flow cytometry data.	Data acquired by FACS Calibur™ was analyzed using BD CellQuest™ Pro Software (BD Biosciences). Data acquired by ImageStream®X was analyzed using IDEAS® Software (AMNIS®). FACS sorting data was assessed using FACS Diva™ Software (BD Biosciences).
8. Describe the abundance of the relevant cell populations within post-sort fractions.	Representative figures provided in Extended Data Figure 10a.
9. Describe the gating strategy used.	For cell sorting, the first gate was set to "viable" cells in FSC/SSC plot, and from those populations of interest were gated in "green vs red" plot (B525/YG582). Positive and negative cell fractions were clearly separable (see Extended Data Figure 10a).

Tick this box to confirm that a figure exemplifying the gating strategy is provided in the Supplementary Information. ☒